Mathematical Biosciences 376 (2024) 109285

Contents lists available at ScienceDirect

Mathematical Biosciences

journal homepage: www.elsevier.com/locate/mbs

Original Research Article

Stoichiometric theory in aquatic carbon sequestration under elevated carbon dioxide

Zhenyao Sun [a,b], Hao Wang [b], Meng Fan [a,*]

[a] School of Mathematics and Statistics, Northeast Normal University, 5268 Renmin Street, Changchun, Jilin, 130024, PR China
[b] Interdisciplinary Lab for Mathematical Ecology and Epidemiology, Department of Mathematical and Statistical Sciences, University of Alberta, Edmonton T6G 2G1, Canada

ARTICLE INFO

Keywords:
Carbon dioxide
Algae-bacteria interaction
Ecological stoichiometry
Carbon sequestration

ABSTRACT

Global climate change projections indicate that the atmospheric concentration of carbon dioxide will increase twofold by the end of this century. However, how the elevated carbon dioxide affects aquatic carbon sequestration and species composition within aquatic microbial communities remains inconclusive. To address this knowledge gap, we formulate a bacteria-algae interaction model to characterize the effects of elevated carbon dioxide on aquatic ecosystems and rigorously derive the thresholds determining the persistence and extinction of algae or bacteria. We explore the impacts of abiotic factors, such as light intensity, nutrient concentration, inorganic carbon concentration and water depth, on algae and bacteria dynamics. The main findings indicate that the elevated atmospheric carbon dioxide will increase algae biomass and thus facilitate carbon sequestration. On the other hand, the elevated atmospheric carbon dioxide will reduce bacterial biomass, and excessive carbon dioxide concentrations can even destroy bacterial communities. Numerical simulations indicate that eutrophication and intensified light intensity can reduce aquatic carbon sequestration, while elevated atmospheric carbon dioxide levels can mitigate eutrophication. Furthermore, higher algae respiration and death rates are detrimental to carbon sequestration, whereas the increased bacterial respiration rates promote carbon sequestration.

1. Introduction

In aquatic ecosystems, algae serve as the primary producers of paramount importance. They perform photosynthesis, supply ample oxygen to aquatic organisms, and are integral to the flow of energy, circulation of materials, and transmission of information within aquatic ecosystems [1,2]. Bacteria, likewise, play a significant role within aquatic communities. They excel in the decomposition of organic matter and perform indispensable roles in the restoration of water quality, thereby contributing to the sustainable development of aquatic ecosystems [3–5].

The interactions between algae and bacteria involve many intricate biological mechanisms, as illustrated in Fig. 1.1. Algae thrive by assimilating nutrients like phosphorus and nitrogen from water while capturing carbon dioxide (CO_2) and sunlight for photosynthesis [6–8]. Moreover, algae exude extra energy in the form of organic carbon. Bacteria, in return, depend on dissolved organic carbon (DOC) as a source of energy and carbon. Consequently, algae serve as a crucial source of DOC for bacteria [9,10]. This establishes a form of bottom-up control over bacteria. In addition to DOC, bacteria survival and proliferation hinge on nutrient availability [1,9], signifying a direct competition between algae and bacteria for these resources. Consequently, algae and bacteria mutually influence each other's growth and biomass density through bottom-up control and competition.

Since the industrial revolution, the Earth's atmosphere has experienced an unprecedented surge in CO_2 concentration, primarily attributed to fossil fuel combustion and deforestation [11]. Specifically, it is reported that CO_2 concentration increased from 288 ppm to 315 ppm between 1800 and 1960, followed by a rise to 400 ppm from 1960 to 2014 [12,13]. With the acceleration of industrialization, climate change models predict a substantial elevation in atmospheric CO_2 levels, with projections estimating an increase to 800–1000 ppm by the end of the 21st century [14,15]. This significant shift is anticipated to have profound repercussions on aquatic microbial communities, as nearly one-third of anthropogenic CO_2 emissions into the atmosphere are ultimately absorbed by the ocean [16,17]. Several researchers have conducted experimental investigations to explore the effects of CO_2 on algal growth. For example, Urabe et al. [18] observed that heightened atmospheric carbon dioxide concentrations increased the

* Corresponding author.
E-mail address: mfan@nenu.edu.cn (M. Fan).

https://doi.org/10.1016/j.mbs.2024.109285
Received 12 May 2024; Received in revised form 16 July 2024; Accepted 19 August 2024
Available online 22 August 2024

partial pressure of carbon dioxide in water, thereby stimulating algal growth. It is noted that the saturation level of algal abundance was notably higher in treatments with increased carbon dioxide, implying that carbon dioxide constrained algae growth in the control group. Moreover, it is found that the final algal cellular quota (P:C) was significantly lower in the elevated carbon dioxide treatments compared to the control treatment. However, theoretical frameworks that predict how increasing CO_2 levels will affect algal growth and the species composition of aquatic communities still need to be developed.

Carbon sequestration involves capturing and storing CO_2 from the atmosphere or other sources, thereby mitigating its release into the atmosphere, where it contributes to the greenhouse effect and global warming [19]. Water bodies such as lakes and oceans are increasingly recognized as vital components of the global carbon cycle [20,21]. This acknowledgment stems from the significant roles played by algae and bacteria in carbon and nutrient cycling in aquatic ecosystems, facilitated by various physiological and biochemical processes [22]. Utilizing algae for CO_2 bio-fixation presents a promising option for sequestration due to their substantially higher CO_2 fixation capacity through photosynthesis and solar utilization efficiency compared to terrestrial plants, as well as their rapid growth rates and tolerance to extreme environments [23]. Indeed, to foster carbon sequestration, it is imperative to understand the influence of elevated atmospheric CO_2 on aquatic carbon sequestration, and it is crucial to elucidate the intricate relationships among algae, bacteria, and abiotic factors, such as nutrient concentration and light intensity.

As a robust framework, ecological stoichiometry integrates energy balance by considering multiple nutrients within ecological systems [24]. Both theoretical ecologists and experimental studies have underscored the significance of ecological stoichiometry. Models founded on ecological stoichiometry are instrumental in elucidating diverse ecological mechanisms and resolving existing paradoxes, such as those observed in producer-grazer systems [25–27], three-species models [28,29], plant and herbivore interactions [30], and the decomposition of organic matter [9]. In [31], Davies and Wang proposed a stoichiometric producer-grazer model incorporating atmospheric CO_2 by extending the WKL model [27]. Their analysis reveals that carbon sequestration resulting from elevated atmospheric CO_2 levels may be constrained by inadequate phosphorus availability. Furthermore, elevated atmospheric CO_2 concentrations lead to a decline in the stoichiometric quality of producers where phosphorus is limiting.

Most lakes are seasonally separated by two distinct layers, epilimnion and hypolimnion [32]. The epilimnion, characterized by warmer temperatures and strong turbulence, constitutes the upper layer and is typically well-mixed. In contrast, the hypolimnion forms the colder, lower layer, that remains relatively undisturbed and receives minimal light penetration. Light enters epilimnion through the water surface and diminishes rapidly with increasing depth [33]. Nutrients from the lake bottom are transported upwards through the hypolimnion to the epilimnion via water exchange mechanisms [8]. DOC is primarily generated by the exudation of algae. For the sake of simplifying the study on how algae stimulate bacterial growth, the external input of DOC is negligible [9].

Algae-bacteria interactions in lakes have been modeled [9,34], but to our knowledge, few studies have considered algae-bacteria interactions limited by atmospheric carbon dioxide (see Fig. 1.1). Given the existing research and the above discussion, this study presents a mathematical model to characterize the interactions of algae and bacteria based on ecological stoichiometry. This stoichiometric model extends the work of Wang et al. [9] by incorporating atmospheric carbon dioxide into the modeling of algae-bacteria interactions in the epilimnion.

The rest of the paper is organized as follows. In Section 2, a new stoichiometric model is formulated to explore the interactions between algae and bacteria. In Section 3, we investigate the algae dynamics.

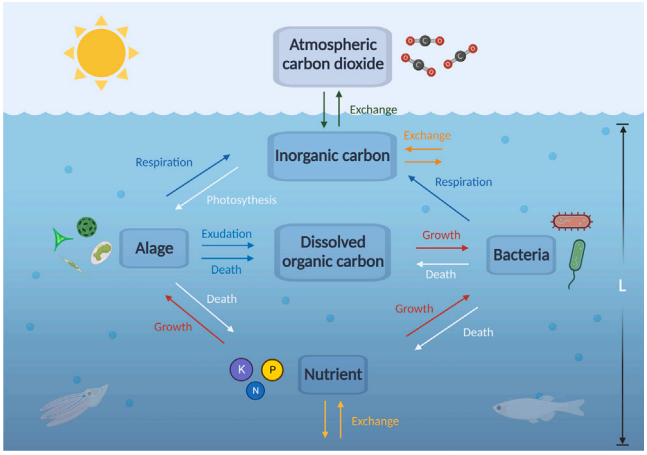

Fig. 1.1. Algae-bacteria interactions in epilimnion. The figure is created with BioRender.com.

Table 2.1
Variables with biological meanings and units in model (2.2).

Variable	Biological meaning	Unit
A	Algal carbon density	mgC/m^3
Q	Algal cell quota (P:C)	mgP/mgC
B	Bacterial density	mgC/m^3
R	Inorganic carbon concentration	mgC/m^3
S	Dissolved organic carbon concentration	mgC/m^3
P	Dissolved phosphorus concentration	mgP/m^3

In Section 4, we explore the algae-bacteria interaction dynamics. According to theoretical analysis and numerical simulations, the effects of elevated carbon dioxide on algae and bacteria in aquatic ecosystems are evaluated under realistic environmental parameters. In Section 5, we examine the impacts of certain biotic factors and the metabolism rates of algae and bacteria on carbon sequestration. Finally, some concluding remarks are presented in Section 6.

2. Model formulation

In this section, we formulate the stoichiometric model to characterize the interactions among algae, algal cell quota, bacteria, dissolved inorganic carbon, dissolved organic carbon, and dissolved nutrients in the water column (see Table 2.1). Assume that the water column has a depth of L, where $x = 0$ represents the water surface, and $x = L$ denotes the bottom of the water column. All parameters and their biological meanings are presented in Table 2.2.

In aquatic ecosystems, algae require nutrients for growth and depend on inorganic carbon and light for photosynthesis. Therefore, algal growth is assumed to be affected by light intensity, dissolved nutrients (in this case, phosphorus), and inorganic carbon availability. This relationship is modeled according to the Droop equation, Monod equation, and Lambert–Beer law. Based on the Lambert–Beer Law [35], the light intensity at a depth x in the water column is given by

$$I(x, A) = I_{in} \exp(-K_{bg} x - kA), \ 0 < x < L.$$

Furthermore, the water column is assumed to be well mixed, then algal depth-averaged growth function includes

$$\bar{I}(A) = \frac{1}{L}\int_0^L \frac{I(x,A)}{I(x,A)+H}\mathrm{d}x = \frac{1}{L(kA+K_{bg})}\ln\left(\frac{H+I_{in}}{H+I(L,A)}\right).$$

Combining the factors mentioned above, the algal growth function is presented below:

$$\mu_a(Q)g_r(R)\bar{I}(A) = r_a\left(1-\frac{Q_{\min}}{Q}\right)\frac{R}{K_r+R}\frac{1}{L}\int_0^L \frac{I(x,A)}{I(x,A)+H}\mathrm{d}x,$$

where $Q_{\min}$ stands for the minimal phosphorus cell quota of algae, K_r is the half-saturation constant for inorganic carbon uptake. The loss of algal biomass is caused by respiration $l_a A$, death $d_a A$, algal sinking v/L, and water exchange D/L at the bottom of the water column. The algal nutrient uptake rate is $\rho(Q)g_a(P)$, where

$$g_a(P) = \frac{P}{K_a + P},\ \rho(Q) = \rho_m \frac{Q_{\max} - Q}{Q_{\max} - Q_{\min}},\ Q_{\min} \le Q \le Q_{\max}.$$

In addition, the dilution rate of algal cell quota is $\mu_a(Q)g_r(R)\bar{I}(A)$.

The growth of heterotrophic bacteria depends on DOC and dissolved phosphorus. The uptake functions of DOC and phosphorus are assumed to take the monod form

$$g_b(P) = \frac{P}{K_b + P},\ g_s(S) = \frac{S}{K_s + S},$$

where K_b and K_s are the half-saturation constant for phosphorus uptake and DOC uptake, respectively. The depletion of bacterial biomass is caused by bacterial respiration $l_b B$, death $d_b B$, and water exchange DB/L.

Remark 1. Based on Fig. 1.1, dissolved phosphorus is essential for the growth of algae and bacteria, and they compete for the limited phosphorus in the water column. In general, bacteria exhibit higher nutrient affinity than algae [22,36]. The primary reason for this is the smaller cell size and, thus, the more excellent surface-area-to-volume ratio in bacteria [22], which allows them to more effectively uptake and utilize available nutrients. In addition, K_a and K_b are the half-saturation constants for algal and bacterial phosphorus uptake, respectively, and a lower half-saturation constant indicates that the species is more efficient at utilizing low concentrations of nutrients. Therefore, $K_a > K_b$ is established throughout this study to indicate that bacteria have higher nutrient affinity than algae.

The variation of inorganic carbon (IC) primarily arises from CO_2 exchange between the air and water. Atmospheric CO_2 can cross the air–water interface to enter the water column. Let gCO_2 represent the carbon dioxide input rate across the air–water interface, related to the carbon dioxide concentration gradient at the water surface. Based on [37], gCO_2 can be determined by the difference between the dissolved carbon dioxide in equilibrium with the atmospheric pressure ($[CO_2^*]$) and the actual dissolved dioxide concentration ($[CO_2]$), which is expressed as

$$g_{CO2} = c([CO_2^*] - [CO_2]) := \alpha R_{in}, \tag{2.1}$$

where c is the exchange rate. Furthermore, $[CO_2^*]$ can be calculated using Henry's Law, namely, $[CO_2^*] = K_0 pCO_2$, where pCO_2 is the partial pressure of CO_2 and K_0 is the solubility constant. Let $\alpha(R_{in} - R)$ represent the IC exchange. Furthermore, algae consume IC for photosynthesis to produce organic matter, with a consumption rate $\mu_a(Q)g_r(R)\bar{I}(A)A$, and both algae and bacteria perform respiration to generate inorganic carbon with rates $l_a A$ and $l_b B$ respectively.

The source of DOC stems from exudation resulting from the photosynthesis of algae and is expressed as

$$\begin{aligned}\mu_s(A,Q,R) &= \left(r_a - \mu_a(Q)\right) g_r(R)\bar{I}(A)A \\ &= r_a A \frac{Q_{\min}}{Q} \frac{R}{K_r + R} \frac{1}{L} \int_0^L \frac{I(x,A)}{I(x,A) + H} \mathrm{d}x.\end{aligned}$$

The death of algae and bacteria also produces DOC, namely $d_a A$ and $d_b B$, respectively. The reduction of DOC is determined by bacterial consumption $r_b g_b(P)g_s(S)B/\gamma$ and water exchange DS/L.

The variations in dissolved phosphorus mainly arise from consumption by algae and bacteria with the consumption rate given by

$$qr_b g_b(P)g_s(S)B + \rho(Q)g_a(P)A,$$

and phosphorus exchange at rate $D(P_{in} - P)/L$. Furthermore, after their death, phosphorus elements are cycled back into the system at the rate $d_a AQ + qd_b B$.

From the above discussion, the following algae-bacteria interaction model is achieved

$$\begin{aligned}
\frac{\mathrm{d}A}{\mathrm{d}t} &= \underbrace{\mu_a(Q)g_r(R)\bar{I}(A)A}_{\text{algae growth}} - \underbrace{l_a A}_{\text{respiration}} - \underbrace{d_a A}_{\text{death}} - \underbrace{\frac{v+D}{L}A}_{\text{sinking and exchange}}, \\
\frac{\mathrm{d}Q}{\mathrm{d}t} &= \underbrace{\rho(Q)g_a(P)}_{\text{replenishment}} - \underbrace{\mu_a(Q)g_r(R)\bar{I}(A)Q}_{\text{dilution due to growth}}, \\
\frac{\mathrm{d}B}{\mathrm{d}t} &= \underbrace{r_b g_b(P)g_s(S)B}_{\text{bacterial growth}} - \underbrace{l_b B}_{\text{respiration}} - \underbrace{d_b B}_{\text{death}} - \underbrace{\frac{D}{L}B}_{\text{exchange}}, \\
\frac{\mathrm{d}R}{\mathrm{d}t} &= \underbrace{\alpha(R_{in} - R)}_{\text{IC input and exchange}} - \underbrace{\mu_a(Q)g_r(R)\bar{I}(A)A}_{\text{IC uptake by algae}} + \underbrace{l_a A + l_b B}_{\text{IC recycling}}, \\
\frac{\mathrm{d}S}{\mathrm{d}t} &= \underbrace{\mu_s(A,Q,R)}_{\text{DOC exudation from algae}} - \underbrace{\frac{1}{\gamma}r_b g_b(P)g_s(S)B}_{\text{bacterial consumption}} + \underbrace{d_a A + d_b B}_{\text{DOC recycling}} - \underbrace{\frac{D}{L}S}_{\text{exchange}}, \\
\frac{\mathrm{d}P}{\mathrm{d}t} &= \underbrace{\frac{D}{L}(P_{in} - P)}_{\text{P input and exchange}} - \underbrace{qr_b g_b(P)g_s(S)B}_{\text{bacterial consumption}} - \underbrace{\rho(Q)g_a(P)A}_{\text{algous consumption}} \\
&\quad + \underbrace{d_a AQ + qd_b B}_{\text{P recycling}}.
\end{aligned} \tag{2.2}$$

Considering the biological significance of model (2.2), the initial values are assumed to satisfy

$$\begin{aligned}&A(0) > 0,\quad Q_{\min} \le Q(0) \le Q_{\max}, \\ &B(0) > 0,\quad R(0) > 0,\quad S(0) > 0,\quad P(0) > 0.\end{aligned} \tag{2.3}$$

Furthermore, for certain initial values satisfying (2.3), there exists a unique positive solution of model (2.2). By standard mathematical arguments, it is not difficult to show that the set

$$\Omega := \left\{ (A,Q,B,R,S,P) \in \mathbb{R}_+^6 \middle| \begin{array}{l} A \ge 0, Q_{\min} \le Q \le Q_{\max}, \\ B \ge 0, R \ge 0, S \ge 0, P \ge 0 \end{array} \right\}$$

is positively invariant with respect to model (2.2).

Theorem 1. *The system (2.2) is dissipative, and the set*

$$\Delta := \left\{ (A,Q,B,R,S,P) \in \Omega \middle| \begin{array}{l} AQ + qB + P \le P_{in}, R \le \frac{P_{in}}{\alpha}\left(\frac{l_a}{Q_{\min}} + \frac{l_b}{q}\right) + R_{in}, \\ S \le \frac{LP_{in}}{D}\left(\frac{r_a + d_a}{Q_{\min}} + \frac{d_b}{q}\right) \end{array} \right\}$$

is a globally attracting region.

Proof. Denote $\Phi = AQ + qB + P$, which represents the total phosphorus in the entire water column. It follows from model (2.2) that

$$\begin{aligned}\frac{\mathrm{d}\Phi}{\mathrm{d}t} &= \frac{D}{L}\left(P_{in} - (AQ + qB + P)\right) - \left(l_a + \frac{v}{L}\right)AQ - ql_b B \\ &\le \frac{D}{L}(P_{in} - \Phi),\end{aligned}$$

which implies

$$\limsup_{t\to\infty} \Phi(t) \le P_{in}.$$

Note that $Q_{\min} \le Q(t) \le Q_{\max}$ and the cell quote of bacteria q, then one has

$$\limsup_{t\to\infty} A(t) \le \frac{P_{in}}{Q_{\min}},\quad \limsup_{t\to\infty} B(t) \le \frac{P_{in}}{q}.$$

For the DOC equation in model (2.2), direct calculation yields that

$$\frac{\mathrm{d}S}{\mathrm{d}t} \le r_a A + d_a A + d_b B - \frac{D}{L}S \le \left(\frac{r_a + d_a}{Q_{\min}} + \frac{d_b}{q}\right)P_{in} - \frac{D}{L}S,$$

then it follows that

$$\limsup_{t\to\infty} S(t) \le \frac{LP_{in}}{D}\left(\frac{r_a + d_a}{Q_{\min}} + \frac{d_b}{q}\right).$$

Table 2.2
Parameters with their biological meanings and units in model (2.2).

Parameter	Biological meaning	Value	Unit	Reference
r_a	Maximum specific growth rate of algae	1	day^{-1}	[1]
$Q_{\min}$	Algal cell quota at which growth ceases	0.004	gP/gC	[9]
K_r	Half-saturation constant for algal inorganic carbon uptake	60	mgC/m^3	[38]
L	Depth of the water column	3 (2–10)	m	[39]
I_{in}	Light intensity at water surface	300	$\mu mol(photons)/(m^2\ s)$	[9]
k	Algal biomass-specific light attenuation coefficient	0.0003	m^2/mgC	[9]
K_{bg}	Background light attenuation coefficient	0.6(0.3–0.9)	m^{-1}	[9]
H	Half-saturation constant for light-limit algal growth	120	$\mu mol(photons)/(m^2\ s)$	[9]
l_a	Respiration rate of algae	0.02	day^{-1}	[40]
d_a	Death rate of algae	0.1	day^{-1}	[41]
ν	Sinking velocity of algae	0.1(0.05–0.25)	m/day	[9]
D	Water exchange rate	0.02	m/day	[9]
ρ_m	Maximum specific nutrient uptake rate of algae	1(0.2–1)	gP/gC/day	[9]
$Q_{\max}$	Algal cell quota at which nutrient uptake ceases	0.04	gP/gC	[9]
K_a	Half-saturation constant for algal nutrient uptake	1.5	mgP/m^3	[42]
r_b	Maximum bacterial growth rate	2.5 (1.5–4)	day^{-1}	[9]
K_b	Half-saturation constant for bacterial nutrient uptake	0.1(0.06–0.4)	mgP/m^3	[9]
K_s	Half-saturation constant for bacterial DOC uptake	100(100–400)	mgC/m^3	[9]
l_b	Respiration rate of bacteria	0.2	day^{-1}	[9]
d_b	Death rate of bacteria	0.1	day^{-1}	[9]
α	Inorganic carbon exchange rate	0.264	day^{-1}	[38]
R_{in}	Inorganic carbon input	150	mgC/m^3	Assumed
γ	C-dependent yield constant for bacterial growth	0.5	–	[9]
P_{in}	Phosphorus input	120	mgP/m^3	[9]
q	Fixed cell quota of bacteria	0.15	maP/mgC	[9]

In addition, considering the IC equation in model (2.2), through similar discussions, it is deduced that

$$\frac{\mathrm{d}R}{\mathrm{d}t} \le \alpha(R_{in}-R)+l_aA+l_bB \le \left(\frac{l_a}{Q_{\min}}+\frac{l_b}{q}\right)P_{in}+\alpha(R_{in}-R),$$

which implies

$$\limsup_{t\to\infty} R(t) \le \frac{P_{in}}{\alpha}\left(\frac{l_a}{Q_{\min}}+\frac{d_b}{q}\right)+R_{in}.$$

Therefore, based on the aforementioned discussions, the set Δ is a globally attracting region and the system (2.2) is dissipative. □

3. Algae dynamics

To explore the dynamical behaviors of model (2.2), we first focus on algae dynamics. Set $B=0$, then model (2.2) reduces to

$$\begin{aligned}
\frac{\mathrm{d}A}{\mathrm{d}t} &= \mu_a(Q)g_r(R)\bar{I}(A)A-l_aA-d_aA-\frac{\nu+D}{L}A := F_1,\\
\frac{\mathrm{d}Q}{\mathrm{d}t} &= \rho(Q)g_a(P)-\mu_a(Q)g_r(R)\bar{I}(A)Q := F_2,\\
\frac{\mathrm{d}R}{\mathrm{d}t} &= \alpha(R_{in}-R)-\mu_a(Q)g_r(R)\bar{I}(A)A+l_aA := F_3,\\
\frac{\mathrm{d}P}{\mathrm{d}t} &= \frac{D}{L}(P_{in}-P)-\rho(Q)g_a(P)A+d_aAQ := F_4.
\end{aligned} \tag{3.4}$$

It is trivial to show that system (3.4) is well-posed and the set

$$\Lambda = \left\{(A,Q,R,P)\in\mathbb{R}^4_+ \,\middle|\, A\ge 0, Q_{\min}\le Q\le Q_{\max}, R\ge 0, P\ge 0\right\}$$

is positively invariant with respect to system (3.4) and is globally attracting.

Direct calculations yield that system (3.4) has following two types of possible stead states: the nutrient-only steady state $E_0=(0,\hat{Q},R_{in},P_{in})$, where

$$\hat{Q}=\frac{\beta(P_{in})Q_{\max}+r_aQ_{\min}g_r(R_{in})\bar{I}(0)}{\beta(P_{in})+r_ag_r(R_{in})\bar{I}(0)} \text{ with } \beta(P)=\frac{\rho_mg_a(P)}{Q_{\max}-Q_{\min}},$$

and the positive steady state $E^*=(\bar{A},\bar{Q},\bar{R},\bar{P})$, where $\bar{A},\bar{Q},\bar{R},\bar{P}$ satisfy

$$\begin{cases}
\mu_a(Q)g_r(R)\bar{I}(A)-l_a-d_a-\dfrac{\nu+D}{L}=0,\\
\rho(Q)g_a(P)-\mu_a(Q)g_r(R)\bar{I}(A)Q=0,\\
\alpha(R_{in}-R)-\mu_a(Q)g_r(R)\bar{I}(A)A+l_aA=0,\\
\dfrac{D}{L}(P_{in}-P)-\rho(Q)g_a(P)A+d_aAQ=0.
\end{cases} \tag{3.5}$$

Define the critical value d_a^* as follows:

$$d_a^*=\mu_a(\hat{Q})g_r(R_{in})\bar{I}(0)-l_a-\frac{\nu+D}{L}.$$

The threshold d_a^* represents the growth rate of algae, which depends on various factors such as the input phosphorus concentration, the input IC concentration, water surface light intensity, the minimum and maximum algal cell quota, and the respiration rate of algae.

Theorem 2. *The positive steady state E^* is unique.*

Proof. From system (3.4), it follows that E^* complies with (3.5). Straightforward simplifications produce

$$\begin{aligned}
P &= P_{in}-\frac{L}{D}\left(l_a+\frac{\nu+D}{L}\right)AQ = P_{in}-\left(\frac{L}{D}l_a+\frac{\nu+D}{D}\right)AQ,\\
R &= R_{in}-\frac{1}{\alpha}\left(\mu_a(Q)g_r(R)\bar{I}(A)-l_a\right)A = R_{in}-\frac{1}{\alpha}\left(d_a+\frac{\nu+D}{L}\right)A.
\end{aligned}$$

Substituting these expressions into the first equation in (3.5) leads to

$$\begin{aligned}
A &= \frac{K_a+P_{in}-\left(\frac{\rho_mP_{in}Q_{\max}}{(l_a+d_a+\frac{\nu+D}{L})(Q_{\max}-Q_{\min})Q}-\frac{\rho_mP_{in}}{(l_a+d_a+\frac{\nu+D}{L})(Q_{\max}-Q_{\min})}\right)}{\frac{L}{D}(l_a+\frac{\nu+D}{L})Q-\left(\frac{\rho_mQ_{\max}\frac{L}{D}(l_a+\frac{\nu+D}{L})}{(l_a+d_a+\frac{\nu+D}{L})(Q_{\max}-Q_{\min})}-\frac{\rho_m\frac{L}{D}(l_a+\frac{\nu+D}{L})Q}{(l_a+d_a+\frac{\nu+D}{L})(Q_{\max}-Q_{\min})}\right)}\\
&:= F(Q).
\end{aligned}$$

Therefore, the first equation in system (3.4) can be expressed as

$$\begin{aligned}
&r_a\left(1-\frac{Q_{\min}}{Q}\right)g_r\left(R_{in}-\frac{1}{\alpha}\left(d_a+\frac{\nu+D}{L}\right)F(Q)\right)\bar{I}(F(Q))\\
&=l_a+d_a+\frac{\nu+D}{L}.
\end{aligned} \tag{3.6}$$

Next, the uniqueness of the positive solution to (3.6) is demonstrated by establishing that $F(Q)$ is decreasing concerning Q. Note that

$$F(x)=\frac{a-(\frac{b}{x}-c)}{dx-(e-fx)}=\frac{(a+c)x-b}{(d+f)x^2-ex},$$

where

$$\begin{aligned}
&a=K_a+P_{in},\ b=\frac{\rho_mP_{in}Q_{\max}}{(l_a+d_a+\frac{\nu+D}{L})(Q_{\max}-Q_{\min})},\\
&c=\frac{\rho_mP_{in}}{(l_a+d_a+\frac{\nu+D}{L})(Q_{\max}-Q_{\min})},\ d=\frac{L}{D}(l_a+\frac{\nu+D}{L}),
\end{aligned}$$

$$e = \frac{\rho_m Q_{\max}\frac{L}{D}(l_a + \frac{\nu+D}{L})}{(l_a + d_a + \frac{\nu+D}{L})(Q_{\max} - Q_{\min})},\ f = \frac{\rho_m \frac{L}{D}(l_a + \frac{\nu+D}{L})}{(l_a + d_a + \frac{\nu+D}{L})(Q_{\max} - Q_{\min})}.$$

Then,

$$F'(x) = \frac{-(a+c)(d+f)x^2 + 2b(d+f)x - be}{((d+f)x^2 - ex)^2} = \frac{G(x)}{((d+f)x^2 - ex)^2}.$$

By simple calculation, one derives that

$$\Delta = [2b(d+f)]^2 - 4(a+c)(d+f)be = 4b(d+f)[b(d+f) - e(a+c)] < 0,$$

since

$$b(d+f) - e(a+c) = -\frac{\rho_m \frac{L}{D}(l_a + \frac{\nu+D}{L})Q_{\max}}{(l_a + d_a + \frac{\nu+D}{L})(Q_{\max} - Q_{\min})}K_a < 0.$$

Then $G(x) = -(a+c)(d+f)x^2 + 2b(d+f)x - be < 0$. Therefore, $F(x)$ is strictly decreasing in x and then the uniqueness of E^* is proved. □

Theorem 3. *The nutrient-only steady state E_0 always exists. If $d_a > d_a^*$, then E_0 is globally asymptotically stable. If $0 < d_a < d_a^*$, then there exists a unique positive steady state E^*, and system (3.4) is uniformly persistent, i.e., there exists an $\epsilon > 0$ such that $\liminf_{t\to\infty} A(t) \geq \epsilon$ for all solutions with $A(0) > 0$.*

Proof. It is obvious that E_0 always exists and the Jacobian matrix at E_0 is

$$J(E_0) = \begin{pmatrix} a_{11} & 0 & 0 & 0 \\ 0 & a_{22} & a_{23} & a_{24} \\ a_{31} & 0 & a_{33} & 0 \\ a_{41} & 0 & 0 & a_{44} \end{pmatrix},$$

where

$$a_{11} = \mu_a(\hat{Q})g_r(R_{in})\bar{I}(0) - l_a - d_a - \frac{\nu + D}{L},$$

$$a_{22} = \frac{\partial \rho}{\partial Q}(\hat{Q})g_a(P_{in}) - r_a g_r(R_{in})\bar{I}(0),$$

$$a_{23} = -\mu_a(\hat{Q})\bar{I}(0)\hat{Q}\frac{\partial g_r}{\partial R}(R_{in}),\ a_{24} = \rho(\hat{Q})\frac{\partial g_a}{\partial P}(P_{in}),$$

$$a_{31} = -\mu_a(\hat{Q})g_r(R_{in})\bar{I}(0) + l_a,$$

$$a_{33} = -\alpha,\ a_{41} = -\rho(\hat{Q})g_a(P_{in}) + d_a\hat{Q},\ a_{44} = -\frac{D}{L}.$$

Note that the eigenvalues of $J(E_0)$ are a_{ii}, $i = 1, \ldots, 4$, and $a_{ii} < 0$, for $i = 2, 3, 4$. Consequently, if $d_a > d_a^*$, i.e., $a_{11} < 0$, then E_0 is locally asymptotically stable.

Subsequently, consider the situation when $0 < d_a < d_a^*$. Recall the definition of the set Λ, define

$$\Lambda_0 = \{(A, Q, R, P) \in \Lambda : A > 0\},$$

and

$$\partial\Lambda_0 := \Lambda \backslash \Lambda_0 = \{(A, Q, R, P) \in \Lambda : A = 0\}.$$

It is straightforward to observe that both Λ_0 and its boundary $\partial\Lambda_0$ are positively invariant for system (3.4), and $\partial\Lambda_0$ is relatively closed within Λ. Moreover, based on Theorem 1, system (3.4) is point dissipative. Let $\Phi(t) : \Lambda \to \Lambda$ denote the solution map of system (3.4), define $M_\partial := \{G \in \partial\Lambda_0 : \Phi(t)G \in \partial\Lambda_0, \forall t \geq 0\}$, and denote by $\omega(G)$ the omega limit set of the trajectory $O^+(G) := \{\Phi(t)G : t \geq 0\}$. Then, one has the following claims.

Claim 1. *$\omega(G) = \{E_0\}$ for any $G \in M_\partial$.*

For any $G \in M_\partial$, one has $\Phi(t)G \in \partial\Lambda_0, t \geq 0$. Consequently $A(t, G) = 0, t \geq 0$. Considering the third and fourth equation in system (3.4), one can derive the following reduced sub-system

$$\begin{cases} \frac{dR}{dt} = \alpha(R_{in} - R), \\ \frac{dP}{dt} = \frac{D}{L}(P_{in} - P). \end{cases}$$

Based on the theory of monotone dynamical system, (R_{in}, P_{in}) is the unique equilibrium of the sub-system, which is globally asymptotically stable. Therefore, it concludes that $\lim_{t\to\infty}(R(t, G), P(t, G)) = (R_{in}, P_{in})$. Moreover, by the theory of asymptotically autonomous semi-flows [43], the equation $Q(t)$ in system (3.4) asymptotically approaches $\hat{Q}$, i.e., $\lim_{t\to\infty} Q(t, G) = \hat{Q}$. Therefore, this claim is established, and E_0 is globally asymptotically stable.

Let $\eta_1 := \frac{1}{2}\left(\mu_a(\hat{Q})g_r(R_{in})\bar{I}(0) - l_a - d_a - \frac{\nu+D}{L}\right) > 0$. Then from the continuity of $\mu_a(Q)$, it follows that there exists a $\sigma_1 > 0$ such that

$$\mu_a(Q)g_r(R_{in})\bar{I}(0) > \mu_a(\hat{Q})g_r(R_{in})\bar{I}(0) - \eta_1,\ \forall |Q - \hat{Q}| < \sigma_1. \tag{3.7}$$

Claim 2. *E_0 is a uniform weak repeller for Λ_0 in the sense that*

$$\limsup_{t\to\infty} |\Phi_t(G) - E_0| \geq \sigma_1,\ \forall S \in \Lambda_0.$$

By the contradiction arguments, assume that there exists a $G \in \Lambda_0$ such that

$$\limsup_{t\to\infty} |\Phi_t(G) - E_0| < \sigma_1.$$

Then, there exists a $\tau_1 > 0$ such that

$$|Q(t, G) - \hat{Q}| < \sigma_1,\ \forall t \geq \tau_1.$$

Combining this with (3.5), one has

$$\begin{aligned} &\mu_a(Q(t, G))g_r(R_{in})\bar{I}(0) - l_a - d_a - \frac{\nu + D}{L} \\ &\quad > \mu_a(\hat{Q})g_r(R_{in})\bar{I}(0) - l_a - d_a - \frac{\nu + D}{L} - \eta_1 = \eta_1, \quad t \geq \tau_1. \end{aligned}$$

Consequently, from the first equation in system (3.4), it follows that

$$\frac{dA(t, G)}{dt} > \eta_1 A(t, G), \quad t \geq \tau_1.$$

Then it implies that $A(t, G)$ is unbounded due to $\eta_1 > 0$, which contradicts to the fact that $\lim_{t\to\infty} A(t, G) = 0$. Hence, Claim 2 holds.

Based on the discussion above, E_0 is isolated in Λ, and the stable set $W(E_0)$ of E_0 satisfies $W(E_0) \cap \Lambda_0 = \emptyset$ [44]. Since $\Phi(t) : \Lambda \to \Lambda$ is point dissipative and compact, there exists a global attractor $\tilde{\Lambda}$ for $\Phi(t)$ [44]. Furthermore, $\Phi(t) : \Lambda \to \Lambda$ is uniformly persistent with respect to $(\Lambda_0, \partial\Lambda_0)$. Then, from [44], it yields that there exists a global attractor $\tilde{\Lambda}_0$ in Λ_0 for Φ_t, and Φ_t admits at least one fixed point $(\bar{A}, \bar{Q}, \bar{R}, \bar{P}) \in \Lambda_0$. Consequently, it follows that $\bar{A} > 0$, $\bar{Q} \geq Q_{\min} > 0$, and $(\bar{R}, \bar{P})$ satisfies

$$\begin{cases} \alpha(R_{in} - \bar{R}) - \mu_a(\bar{Q})g_r(\bar{R})\bar{I}(\bar{A})\bar{A} + l_a\bar{A} = 0, \\ \frac{D}{L}(P_{in} - \bar{P}) - \rho(\bar{Q})g_a(\bar{P})\bar{A} + d_a\bar{A}\bar{Q} = 0. \end{cases}$$

Direct calculation confirms that $\bar{A} > 0$ ensures $\bar{R} > 0$ and $\bar{P} > 0$. Thus, $(\bar{A}, \bar{Q}, \bar{R}, \bar{P})$ is a positive steady-state for (3.4). The proof is complete. □

Theorem 4. *The positive steady state $E^* = (\bar{A}, \bar{Q}, \bar{R}, \bar{P})$ is locally asymptotically stable if $a_0, a_1, a_2 > 0$, and $a_1a_2a_3 > a_1^2 + a_3^2a_0$, where a_i (for $i = 0, 1, 2, 3$) are defined in the proof.*

Proof. The Jacobian matrix of system (3.4) at $E^* = (\bar{A}, \bar{Q}, \bar{R}, \bar{P})$ is

$$J(E^*) = \begin{pmatrix} J_{11} & J_{12} & J_{13} & 0 \\ J_{21} & J_{22} & J_{23} & J_{24} \\ J_{31} & J_{32} & J_{33} & 0 \\ J_{41} & J_{42} & 0 & J_{44} \end{pmatrix},$$

where

$$J_{11} = \mu_a(\bar{Q})g_r(\bar{R})\frac{\partial \bar{I}}{\partial A}(\bar{A})\bar{A} < 0, J_{12} = \frac{\partial \mu_a}{\partial Q}(\bar{Q})g_r(\bar{R})\bar{I}(\bar{A})\bar{A} > 0,$$

$$J_{13} = \frac{\partial g_r}{\partial R}(\bar{R})\mu_a(\bar{Q})\bar{I}(\bar{A})\bar{A} > 0, J_{21} = -\mu_a(\bar{Q})g_r(\bar{R})\frac{\partial \bar{I}}{\partial A}(\bar{A})\bar{Q} > 0,$$

$$J_{22} = \frac{\partial \rho}{\partial Q}(\bar{Q})g_a(\bar{P}) - \mu_a(\bar{Q})g_r(\bar{R})\bar{I}(\bar{A}) - \frac{\partial \mu_a}{\partial Q}(\bar{Q})g_r(\bar{R})\bar{I}(\bar{A})\bar{Q} < 0,$$

$$J_{23} = -\mu_a(\bar{Q})\frac{\partial g_r}{\partial R}(\bar{R})\bar{I}(\bar{A})\bar{Q} < 0, J_{24} = \rho(\bar{Q})\frac{\partial g_a}{\partial P}(\bar{P}) > 0,$$

$$J_{31} = -\mu_a(\bar{Q})g_r(\bar{R})\frac{\partial \bar{I}}{\partial A}(\bar{A})\bar{A} - \mu_a(\bar{Q})g_r(\bar{R})\bar{I}(\bar{A}) + l_a,$$

$$J_{32} = -\frac{\partial \mu_a}{\partial Q}(\bar{Q})g_r(\bar{R})\bar{I}(\bar{A})\bar{A} < 0, J_{33} = -\alpha - \mu_a(\bar{Q})\frac{\partial g_r}{\partial R}(\bar{R})\bar{I}(\bar{A})\bar{A} < 0,$$

$$J_{41} = -\rho(\bar{Q})g_a(\bar{P}) + d_a\bar{Q} < 0, J_{42} = -\frac{\partial \rho}{\partial Q}(\bar{Q})g_a(\bar{P})\bar{A} + d_a\bar{A} > 0,$$

$$J_{44} = -\frac{D}{L} - \rho(\bar{Q})\frac{\partial g_a}{\partial P}(\bar{P})\bar{A} < 0.$$

The characteristic equation of the Jacobian matrix $J(E^*)$ is given by

$$\lambda^4 + a_3\lambda^3 + a_2\lambda^2 + a_1\lambda + a_0 = 0,$$

where

$$a_3 = -(J_{11} + J_{22} + J_{33} + J_{44}) > 0,$$

$$\begin{aligned} a_2 =& J_{11}J_{22} + J_{11}J_{33} + J_{22}J_{44} + J_{33}J_{44} + J_{11}J_{44} \\ & - J_{22}J_{33} - J_{23}J_{32} - J_{12}J_{21} - J_{13}J_{31} - J_{24}J_{42}, \end{aligned}$$

$$\begin{aligned} a_1 =& J_{11}J_{22}J_{33} + J_{22}J_{33}J_{44} + J_{11}J_{23}J_{32} + J_{23}J_{32}J_{44} - J_{11}J_{22}J_{44} \\ & - J_{11}J_{33}J_{44} + J_{12}J_{21}J_{33} - J_{12}J_{23}J_{31} + J_{12}J_{21}J_{44} - J_{13}J_{21}J_{32} \\ & J_{13}J_{22}J_{31} + J_{13}J_{31}J_{44} - J_{12}J_{24}J_{41} + J_{12}J_{24}J_{42} + J_{24}J_{33}J_{42}, \end{aligned}$$

$$\begin{aligned} a_0 =& - J_{11}J_{22}J_{33}J_{44} - J_{11}J_{23}J_{32}J_{44} - J_{12}J_{21}J_{33}J_{44} + J_{12}J_{23}J_{31}J_{44} \\ & + J_{13}J_{21}J_{32}J_{44} - J_{13}J_{22}J_{31}J_{44} - J_{11}J_{24}J_{33}J_{42} + J_{12}J_{24}J_{33}J_{41} \\ & + J_{13}J_{24}J_{31}J_{42} - J_{13}J_{24}J_{32}J_{41}. \end{aligned}$$

By Routh–Hurwitz criterion, $E^* = (\bar{A}, \bar{Q}, \bar{R}, \bar{P})$ is locally asymptotically stable if $a_0, a_1, a_2 > 0$, and $a_1a_2a_3 > a_1^2 + a_3^2a_0$. □

Theorem 5. *System (3.4) undergoes a transcritical bifurcation around E_0 at $d_a = d_a^* = \mu_a(\hat{Q})g_r(R_{in})\bar{I}(0) - l_a - \frac{v+D}{L}$.*

Proof. Selecting d_a as the bifurcation parameter, the theorem is demonstrated by applying Sotomayor's theorem as outlined in [45]. Sotomayor's theorem necessitates that one of the eigenvalues of $J(E_0)$ must equate to zero. The eigenvectors corresponding to the zero eigenvalue of $J(E_0)$ and $J(E_0)^{\mathrm{T}}$ are

$$V = \begin{pmatrix} -\frac{a_{33}}{a_{31}} \\ -\frac{a_{23}}{a_{22}} + \frac{a_{23}a_{33}a_{41}}{a_{22}a_{31}a_{44}} \\ 1 \\ -\frac{a_{33}a_{41}}{a_{31}a_{44}} \end{pmatrix}, W = \begin{pmatrix} 1 \\ 0 \\ 0 \\ 0 \end{pmatrix}.$$

Direct calculation yields that

$$\Delta_1 = W^{\mathrm{T}} \cdot F_{d_a}(E_0; d_a^*) = 0,$$

$$\Delta_2 = W^{\mathrm{T}} \cdot [DF_{d_a}(E_0; d_a^*)V] = \frac{a_{33}}{a_{31}} \neq 0,$$

$$\Delta_3 = W^{\mathrm{T}} \cdot [D^2F(E_0; d_a^*)(V, V)] \neq 0,$$

where $F = (F_1, F_2, F_3, F_4)^{\mathrm{T}}$. According to Sotomayor's theorem, system (3.4) displays a transcritical bifurcation near E_0 when $d_a = d_a^*$. This concludes the proof. □

Fig. 3.2 depicts the time-series solution of system (3.4) with different depths. It is observed that, for $L = 2, 3, 5$, algae thrive in the water column, while algae become extinct when $L = 8$. Notably, algal abundance does not negatively correlate with depth, which contrasts with the findings in [9], despite the lower average sunlight intensity in deeper water columns. This discrepancy arises due to the fact that algal growth necessitates a balanced interaction among sunlight, phosphorus, and IC. Furthermore, the algal cell quota positively correlates with water column depth. Specifically, the eventual IC concentration is relatively high in deep water columns and is low in shallow ones. Moreover, a bifurcation diagram with the algal death rate being the bifurcation parameter is presented in Fig. 3.3, which substantiates the previous theoretical findings. Specifically, when the algal death rate is low, i.e., $d_a < d_a^*$, E_0 becomes unstable, and a unique steady state E^* emerges, indicating algal survival in the aquatic environment. Although the stability of E^* has not yet to be confirmed, numerical simulations support its existence. Conversely, when $d_a > d_a^*$, the substantial loss rate results in algal extinction. In such a scenario, there is no positive steady state, and the nutrient-only steady state E_0 is globally asymptotically stable.

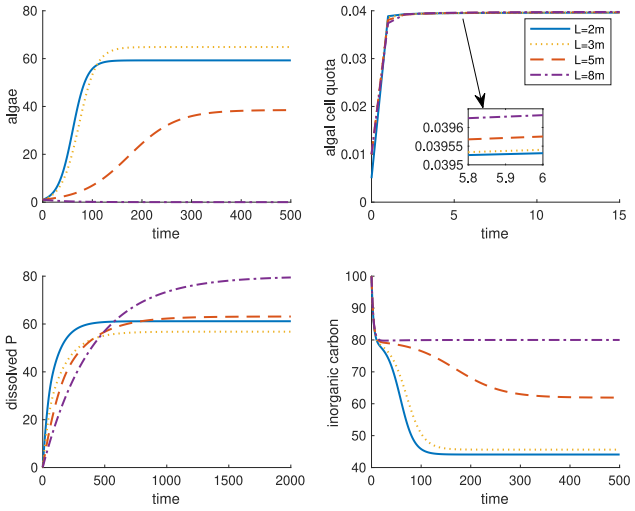

Fig. 3.2. Dynamics of algae without bacteria with varying water column depths L. The parameter values take from Table 2.2 except for $P_{in} = 80$ and $R_{in} = 80$.

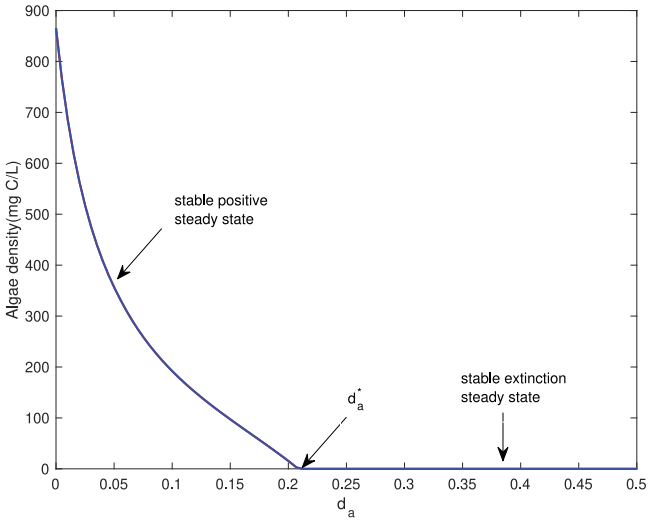

Fig. 3.3. Bifurcation diagram of algae without bacteria with algae death rate d_a being the bifurcation parameter. The parameter values are selected from Table 2.2.

Next, the effect of various abiotic factors on algal density is examined and one parameter bifurcation diagrams are provided for algae. In aquatic ecosystems, three crucial abiotic factors affecting algal growth are the concentration of phosphorus input (P_{in}), the concentration of IC input (R_{in}), and water surface light intensity (I_{in}). Fig. 3.4(a) clearly illustrates that the equilibrium algal density increases with the

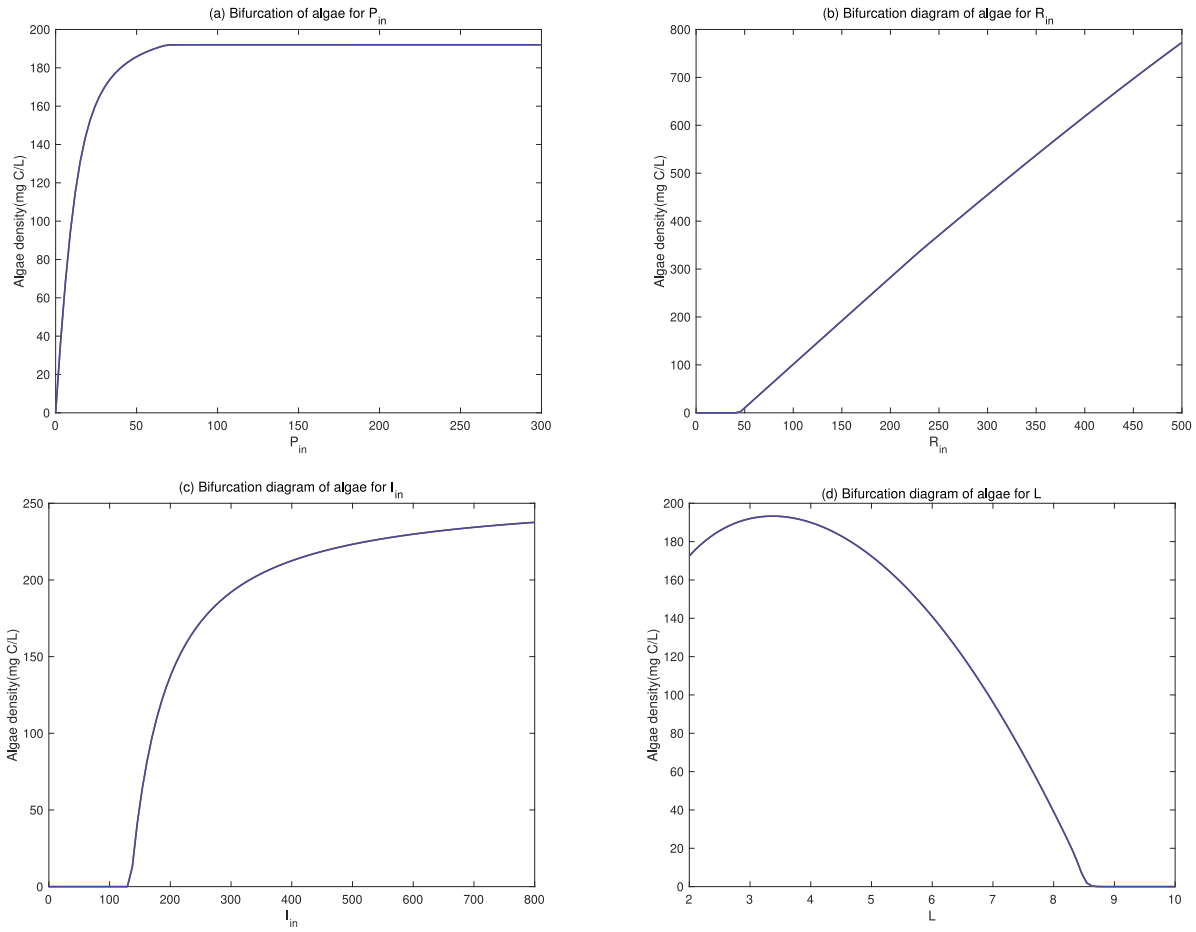

Fig. 3.4. Bifurcation diagram of algae with respect to different abiotic factors. The parameters are from Table 2.2.

increasing levels of total phosphorus input concentration (P_{in}). Higher phosphorus concentrations significantly enhance algal growth on a large scale. Nevertheless, it is worth noting that the cell quota of algae imposes limitations on their growth. It is observed in Fig. 3.4(b) and (c) that the equilibrium algal density increases with increasing inorganic carbon input and light intensity. Elevated carbon dioxide levels stimulate algal growth, and higher light intensity plays a substantial role in the frequent occurrence of algal blooms during summer. However, it is important to note that the critical thresholds exist for inorganic carbon input and light intensity. Beyond these thresholds, for example, if the algal death rate (d_a) surpasses a certain threshold (d_a^*), algae begin to decline gradually. Fig. 3.4(d) reveals that, when algae are affected by multiple abiotic factors, the most suitable depth for algae to thrive is not necessarily at the water's surface. Instead, there exists an optimal depth within the water column for algal growth.

Subsequently, the effects of different abiotic factors and depth on algal growth are considered. The phosphorus input P_{in} is closely related to the eutrophication of the water body, and increasing inorganic carbon input R_{in} characterizes the elevated atmospheric CO_2. For different phosphorus input (see Fig. 3.5(a)), there is an optimal depth of water body for algal survival under the influence of light intensity. What is more, even with higher phosphorus inputs, algae become extinct in deep lakes ($L > 8.7$ m) due to lower average light intensity in the water column. This also explains why shallow lakes are more prone to algae blooms. In Fig. 3.5(b), for the low IC input ($R_{in} = 40$), algae cannot survive in the water column, because IC is one of the important raw materials for algae photosynthesis. As IC concentration increases, algal biomass increases and algae can survive in deeper water bodies. This also shows that the increase in atmospheric CO_2 will stimulate the growth of algae, causing an increase in algal biomass.

Light intensity I_{in} is one of the critical regulators of photosynthesis and metabolism in algae. In Fig. 3.6(a), algae become extinct under low light intensities (e.g., $I_{in} = 100$). As light intensity increases, algae can survive in deeper water bodies. It can be seen that light is an important factor affecting whether algae can survive in deep waters. What is more, the background light attenuation coefficient K_{bg} describes the transmittance of water quality. As K_{bg} decreases, not only can algae survive in deep waters, but also algal biomass increases. As a result, clear shallow lakes are more prone to algae blooms.

The parameter space is explored by performing an uncertainty analysis using a Latin hypercube sampling (LHS) method. Sensitivity analysis is performed by evaluating partial rank correlation coefficients (PRCCs) for various input parameters against output variables over time, and then the key parameters are determined. The result illustrated in Fig. 3.7 suggests that, $\bar{A}$ is more sensitive to r_a, d_a, ν, L, and K_{bg}, followed by $Q_{\min}$, l_a, α, and K_a, among which ν, L, and K_{bg} are closely related to the water environment. As a results, clear shallow lakes with slower water flow are more conducive to the growth of algae.

4. Bacteria-algae interaction dynamics

This section reverts to the original bacteria-algae system described by model (2.2). The system (2.2) may have three types of equilibria:

the extinction steady state $e_0 = (0, \hat{Q}, 0, R_{in}, 0, P_{in})$,

the algae only steady state $e_1 = (\bar{A}, \bar{Q}, 0, \bar{R}, \bar{S}, \bar{P})$,

the coexistence steady state(s) $e^* = (A^*, Q^*, B^*, R^*, S^*, P^*)$.

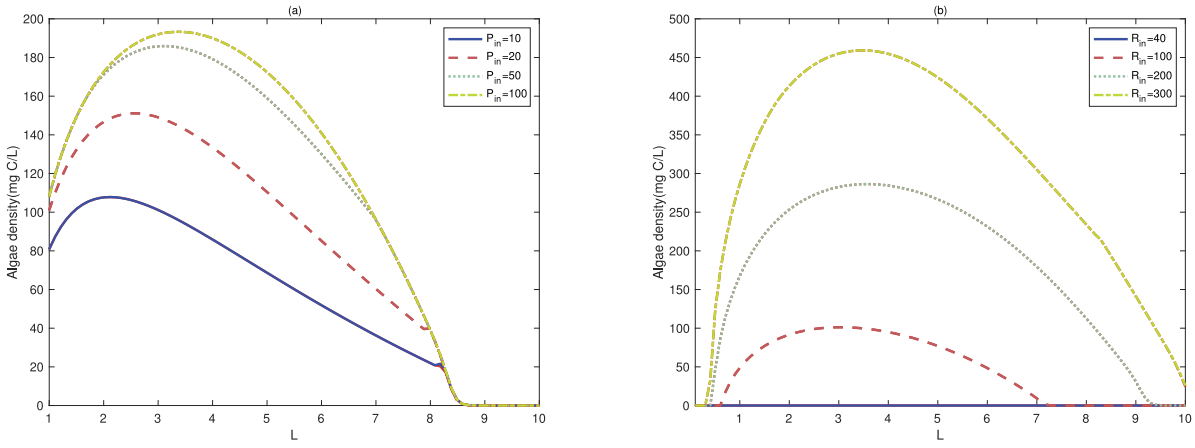

Fig. 3.5. Effects of phosphorus input and inorganic carbon input on algal density.

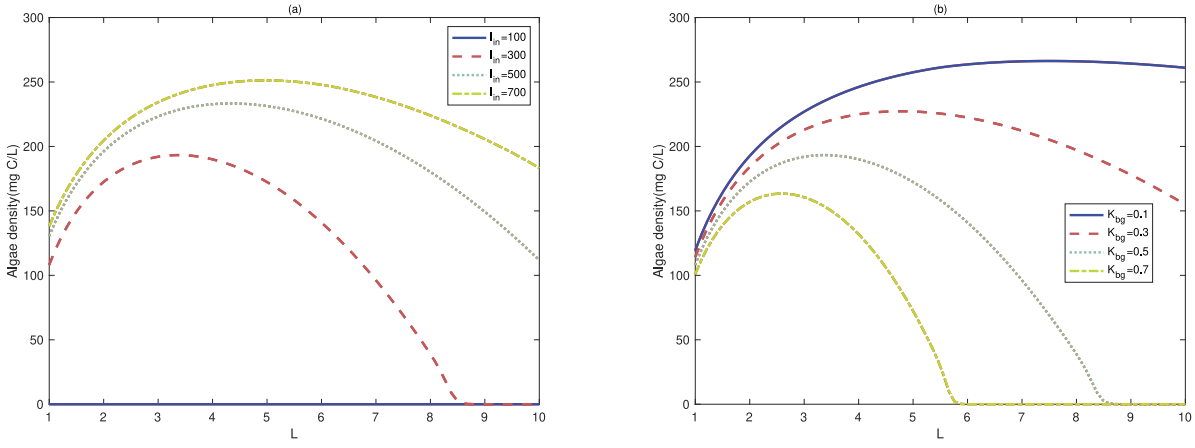

Fig. 3.6. Effects of light input and background light attenuation coefficient on algal density.

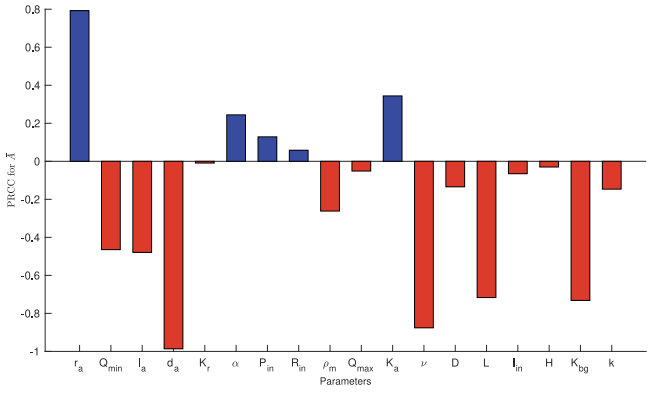

Fig. 3.7. PRCCs of algal density $\bar{A}$ with respect to model parameters.

The bacterial survival threshold, denoted as d_b^*, can be computed by linearizing system (2.2) at e_1. This threshold is given by

$$d_b^* = r_b g_b(\bar{P}) g_s(\bar{S}) - l_b - \frac{D}{L},$$

where $\bar{S} = \frac{D}{L}(\mu_s(\bar{A}, \bar{Q}, \bar{R}) + d_a\bar{A})$ and $\bar{A}, \bar{Q}, \bar{P}$, and $\bar{R}$ are components of E^* of the system (3.4).

A straightforward sufficient criterion for the extinction of both algae and bacteria is presented in the following theorem.

Theorem 6. *If $r_a\bar{I}(0) < D/L$, then both algae and bacteria will be extinct, that is, $\lim_{t\to\infty} A(t) = \lim_{t\to\infty} B(t) = 0$ for all nonnegative initial conditions.*

It is readily apparent that, if $r_a\bar{I}(0) < D/L$, then $d_a > d_a^*$. Consequently, algae and bacteria will become extinct, and the details of the proof are foregone for conciseness.

Employing analogous arguments to those presented in Theorem 3, we establish the stability of the boundary steady states of system (2.2).

Theorem 7. *The extinction steady state e_0 always exists, and it is globally asymptotically stable if $d_a > d_a^*$ and $d_b > d_b^*$. The algae only steady state e_1 exists and is unique if $0 < d_a < d_a^*$ and $d_b > d_b^*$.*

According to the above model analysis, the parameters (d_a, d_b) plane is divided into

$$\begin{aligned} \Gamma_1 &:= \{(d_a, d_b) : d_a > d_a^*\}, \\ \Gamma_2 &:= \{(d_a, d_b) : 0 < d_a < d_a^*,\ d_b > d_b^*\}, \\ \Gamma_3 &:= \{(d_a, d_b) : 0 < d_a < d_a^*,\ 0 < d_b < d_b^*\}. \end{aligned} \tag{4.8}$$

As a result of the presence of P_{in}, the system will not be completely extinct. The extinction of algae and bacteria is inevitable if the algal loss rate d_a is larger than d_a^* regardless of the value of d_b, which is indicated by theoretical analysis and numerical simulations. This is because the organic carbon released by the photosynthesis of algae is an essential resource for bacterial growth. Hence, the extinction of algae will cause the extinction of bacteria, indicating bottom-up control of bacteria by algae (see Fig. 4.8).

Numerical simulations are presented to explore algae-bacteria interaction dynamics. Fig. 4.9 illustrates the impact of changes in algal

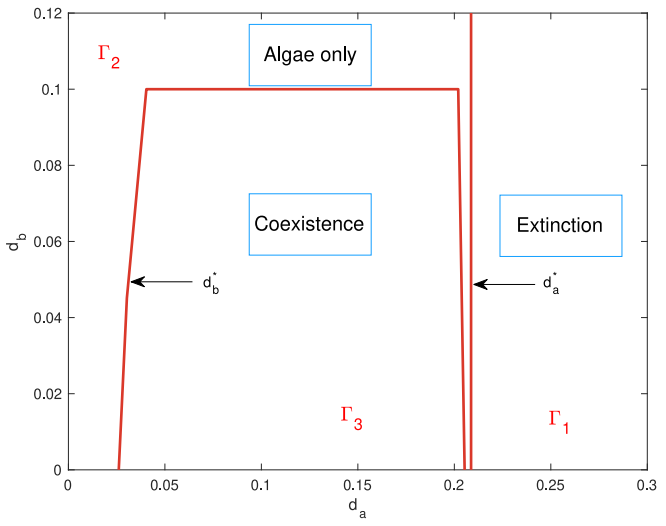

Fig. 4.8. Parameter ranges in the (d_a, d_b) plane with different extinction/existence scenarios. Γ_i, $i = 1, 2, 3$ are defined in (4.8), d_a^* is a critical threshold for algae invasion, and d_b^* is a critical threshold for bacteria invasion when algae exist.

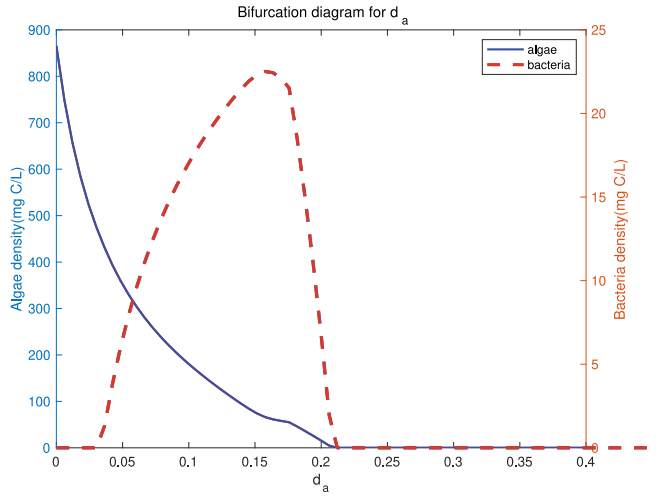

Fig. 4.9. Bifurcation diagram of algae and bacteria $d_a \in (0, 0.4)$. The figure shows the influence of algal density changes on bacterial biomass density by a bottom-up control and competition.

biomass density on bacterial biomass density through bottom-up control and competition. Initially, algae exhibit a low death rate and compete with bacteria for nutrients. Consequently, insufficient nutrient availability leads to d_b surpassing d_b^*, resulting in bacterial extinction. The branching points for algae and bacteria are identical, as they are determined by the same condition where d_a equals d_a^*. The presence of d_b^* does not alter this branching point because d_b^* is defined only if $d_a < d_a^*$.

The impacts of phosphorus input and IC input on both algae and bacteria are investigated. In Fig. 4.10, combined with (a) and (b), both algae and bacteria exhibit an increase concerning the total phosphorus input P_{in}. Higher concentrations of nutrients can alleviate competition between algae and bacteria for nutrients, thereby promoting an increase in bacterial biomass. In Fig. 4.10(a), where the algal death rate is low (i.e., $d_a = 0.1$), the bacterial population cannot survive in the water column when $P_{in} < 40$, even though bacteria exhibit higher nutrient affinity than algae. This is because, besides phosphorus, DOC is also essential for bacterial growth. When $P_{in} < 40$, the DOC produced by algae is insufficient to sustain bacterial growth and metabolism (i.e., bacterial respiration), leading to the extinction of bacteria. However, in Fig. 4.10(b), where the algal death rate is high ($d_a = 0.2$), algae and bacteria can coexist even in oligotrophic environments. This is because when algae die, their cells lyse, releasing substantial amounts of organic matter, including DOC and phosphorus. These organic substances can be utilized by bacteria, promoting their growth and reproduction [46,47]. In particular, when $P_{in} > 50$, the equilibrium densities of algae and bacteria remain constant, indicating that phosphorus concentration is no longer the limiting factor for biomass production.

Fig. 4.10(c) shows the comparison of phosphorus content within algae and bacteria under different values of d_a and P_{in}. The red hollow circles indicate that the phosphorus content within algae is higher than that within bacteria, while the blue solid circles indicate that the phosphorus content within bacteria is higher than that within algae. As shown in Fig. 4.10(c), when d_a is low, the phosphorus content within algae is generally higher than that within bacteria (indicated by red hollow circles). This is because the DOC produced by algae through photosynthesis and cell lysis limits bacterial growth. As d_a increases, the DOC and nutrients released from lysed algae cells increase, which bacteria can utilize, thereby causing the phosphorus content within bacteria to gradually exceed that within algae (indicated by blue solid circles). Fig. 4.10(d) illustrates that only moderate IC input is conducive to bacterial growth. Lower and higher IC levels are detrimental to bacterial populations. The reason behind this observation lies in the fact that DOC and nutrients are two essential resources for bacterial growth. Lower IC input reduces the production of DOC by algae. Conversely, higher inorganic carbon input causes a rapid surge in algal biomass, leading to increased nutrient consumption, which negatively affects bacterial growth.

We examine the influence of water surface light intensity and water depth on both algae and bacteria. In Fig. 4.11(a), a critical value emerges for both algae and bacteria with algae density increasing in response to higher water surface light intensity. Initially, as light intensity rises, bacterial density also increases due to the organic matter produced by the algae. However, with continued increases in light intensity, bacterial density gradually diminishes until it reaches extinction. This phenomenon arises from the excessive blooming of algae in intense light conditions, leading to competition with bacteria for limited nutrients. Consequently, high light intensity, in addition to high IC input, can be detrimental to bacterial populations. As depicted in Fig. 4.11(b), algae tend to thrive at moderate depths of water, while bacteria prefer shallower water bodies. Simultaneously, in deeper water bodies (e.g., $L > 8.6$), the algal population diminishes due to insufficient light availability, and the bacterial population declines along with algae.

Several bifurcation surface diagrams (Figs. 4.12–4.15) are produced to illustrate the densities of algae and bacteria along gradients of abiotic factors. IC serves as the primary substrate for algae photosynthesis, and sufficient light is an indispensable requirement for this process. As shown in Fig. 4.12, an increase in both light intensity (I_{in}) and IC input (R_{in}) progressively stimulates algal growth. However, Fig. 4.13 reveals that the bacterial population can only thrive under moderate levels of I_{in} and R_{in}. Excessive light intensity and inorganic carbon concentrations have a detrimental effect on bacterial population. The reason is that bacterial growth requires a supply of nutrients and organic carbon. When nutrient concentration remains constant, elevated light intensity and inorganic carbon levels lead to an increase in algae density. While this results in the production of more organic carbon, it also escalates nutrient consumption by the growing algae, thereby constraining bacterial growth. From Figs. 4.14 and 4.15, it is evident that, when $L < 8.2$, the augmentation of phosphorus concentration P_{in} fosters the growth of both algae and bacteria. This phenomenon can be attributed to increased P_{in}, which alleviates the competition between algae and bacteria.

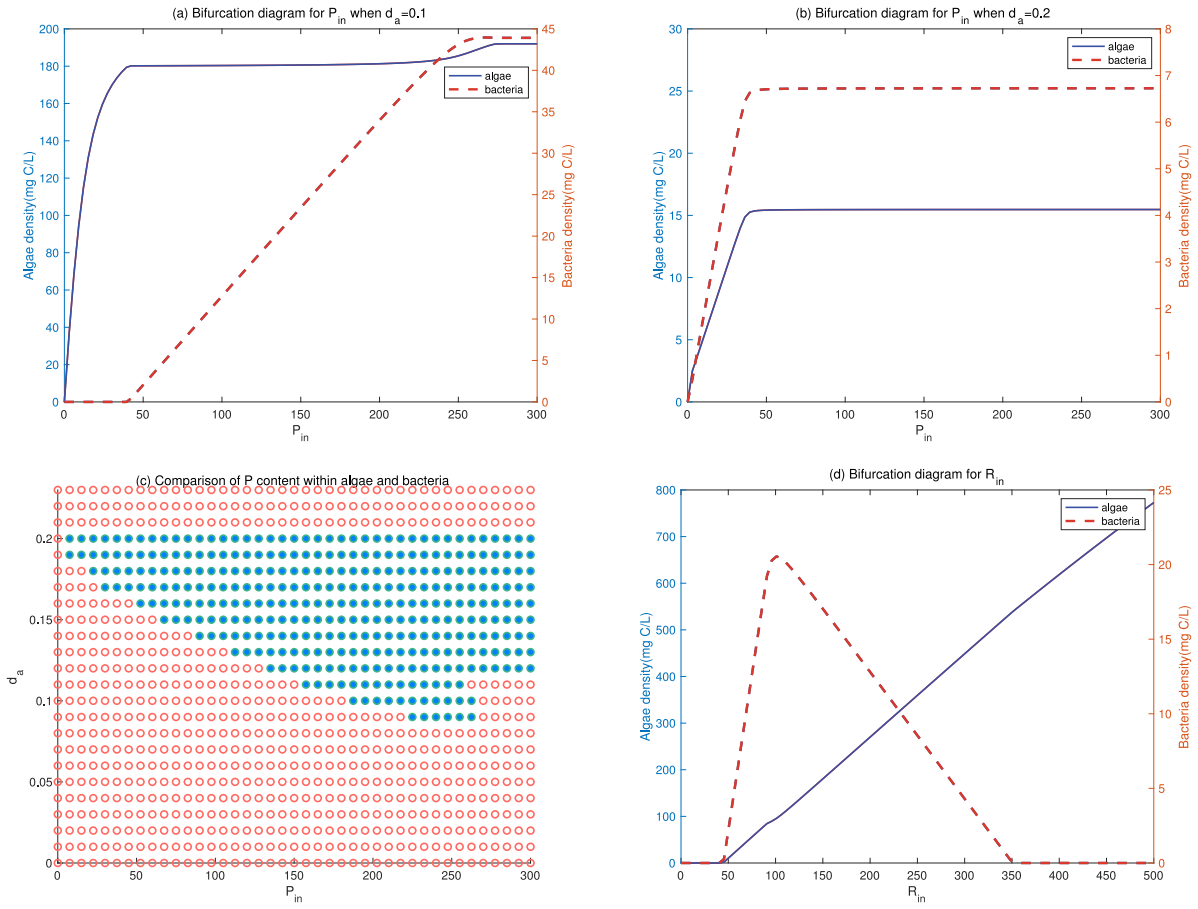

Fig. 4.10. Bifurcation diagrams of algae and bacteria for $P_{in} \in (0, 300)$ and $R_{in} \in (0, 500)$. Panel (a) shows the bifurcation diagram for P_{in} when $d_a = 0.1$. Panel (b) presents the bifurcation diagram for P_{in} when $d_a = 0.2$. Panel (c) compares the phosphorus content within algae and bacteria under different values of d_a and P_{in}, where red hollow circles indicate higher phosphorus content in algae and blue solid circles indicate higher phosphorus content in bacteria. Panel (d) shows the bifurcation diagram for R_{in}. Other parameters are from Table 2.2.

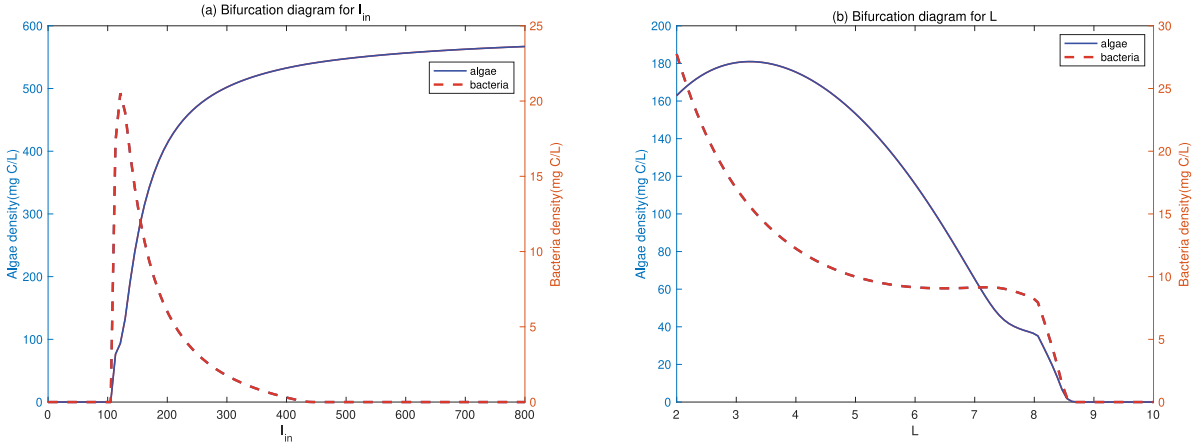

Fig. 4.11. Bifurcation diagrams of algae and bacteria for $I_{in} \in (0, 800)$ and $L \in (2, 10)$.

5. Carbon sequestration

In most aquatic ecosystems, DOC constitutes the largest pool of reduced organic carbon [48], and its concentration serves as a measurable indicator of carbon sequestration. This section will utilize numerical simulations to investigate the influence of both abiotic factors, including phosphorus concentration, inorganic carbon concentration, light intensity, and water depth, as well as biotic factors, such as the respiration and mortality rates of algae and bacteria, on carbon sequestration.

5.1. Abiotic factors

Initially, the effect of phosphorus input P_{in} and IC input R_{in} on carbon sequestration is explored, as illustrated by the bifurcation surface and contour plot in Fig. 5.16. Detailed analyses of this figure

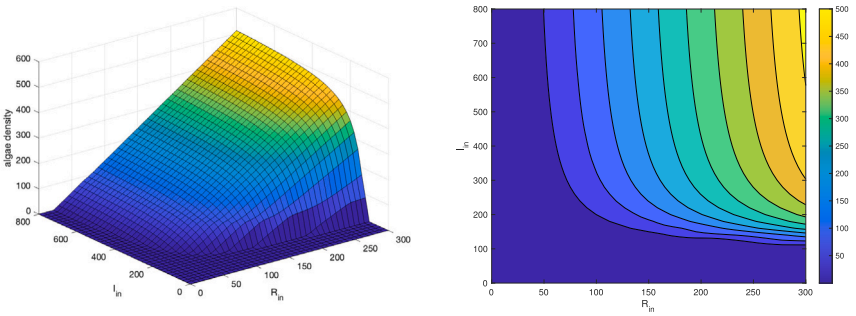

Fig. 4.12. Bifurcation surface and contour plot of algae density for $I_{in} \in (0, 800)$ and $R_{in} \in (0, 300)$.

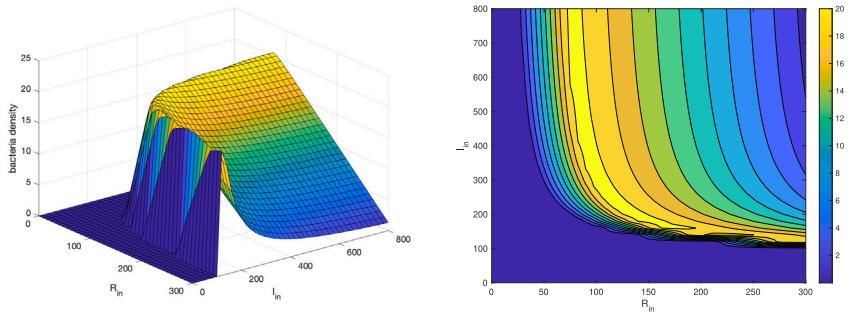

Fig. 4.13. Bifurcation surface and contour plot of bacteria density for $R_{in} \in (0, 300)$ and $I_{in} \in (0, 800)$.

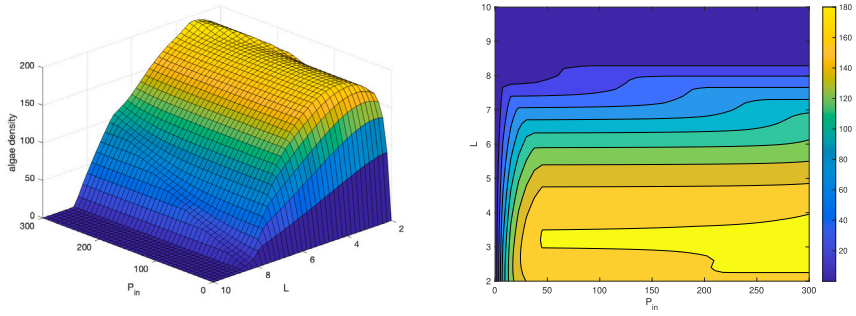

Fig. 4.14. Bifurcation surface and contour plot of algae density for $P_{in} \in (0, 300)$ and $L \in (2, 10)$.

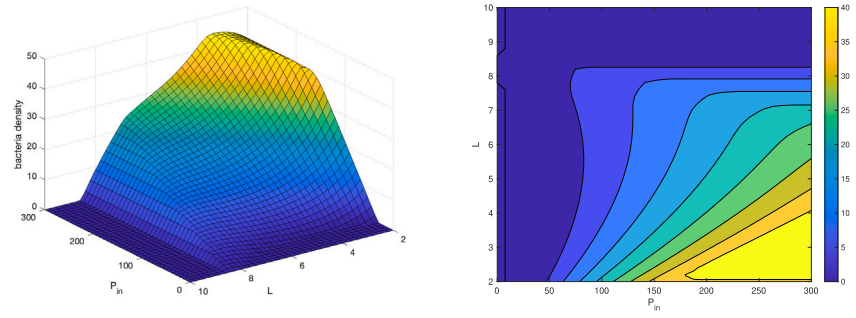

Fig. 4.15. Bifurcation surface and contour plot of bacteria density for $P_{in} \in (0, 300)$ and $L \in (2, 10)$.

unequivocally reveal that, when P_{in} is kept constant, an increase in R_{in} leads to an increase in DOC concentration. This phenomenon arises because heightened atmospheric CO_2 levels result in more CO_2 entering the water, stimulating algae photosynthesis, and generating more DOC, which implies that elevated atmospheric CO_2 facilitates carbon sequestration.

However, when R_{in} is held constant, an increase in P_{in} correlates with a decrease in DOC concentration. This observation suggests that

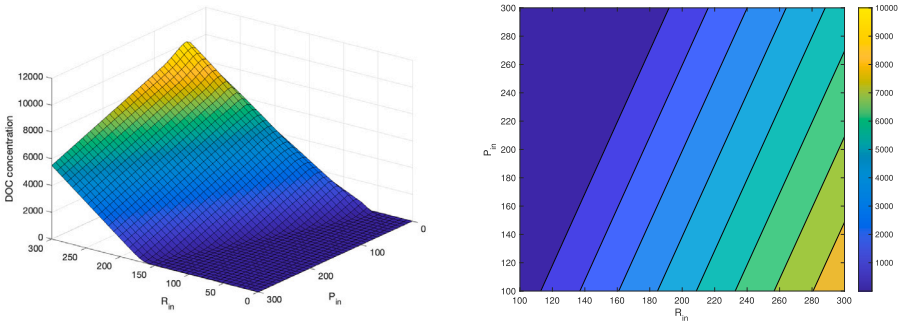

Fig. 5.16. Bifurcation surface and contour plot of DOC concentration for $P_{in} \in (0, 300)$ and $R_{in} \in (0, 300)$.

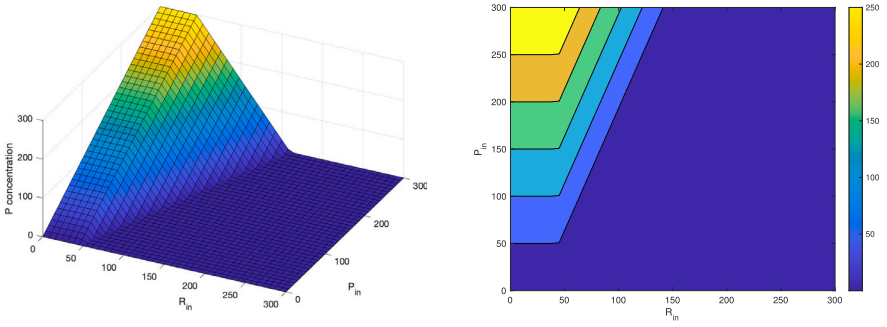

Fig. 5.17. Bifurcation surface and contour plot of P concentration for $P_{in} \in (0, 300)$ and $R_{in} \in (0, 300)$.

eutrophication can decrease carbon sequestration, which is consistent with the finding of Jiang et al. [49]. The reason is that eutrophication alleviates the competition for nutrients between algae and bacteria. Although the DOC produced by algae increases, bacterial growth simultaneously consumes DOC and hence reduces carbon sequestration.

Furthermore, phosphorus (P) is an essential element for all life forms, and many aquatic ecosystems globally have been adversely affected by P eutrophication [50]. Building upon the preceding discussion, the bifurcation surfaces and contour plots of P concentration (see Fig. 5.17) are constructed to investigate the relationship between elevated CO_2 levels and phosphorus. In Fig. 5.17, it is evident that, for specific R_{in} values, an increase in P_{in} leads to a rise in P concentration in the water body. However, when P_{in} is constant, an increase in R_{in} decreases P concentration. This trend arises because the elevated CO_2 levels stimulate algal growth, increasing P consumption. Thus, the elevated atmospheric CO_2 levels can potentially mitigate eutrophication in water bodies [51,52], which is one positive side-effect amidst the otherwise negative impact of anthropogenic CO_2 emissions.

We investigate the effect of water surface light input I_{in} and water depth L on carbon sequestration. As depicted in Fig. 5.18, when L holds constant, an increase in I_{in} corresponds to a rise in DOC concentration. This phenomenon occurs because the heightened light intensity facilitates algae photosynthesis, increasing DOC production. Furthermore, when I_{in} is fixed, the trend of DOC concentration varies with depth L. Initially, there is an increase in DOC concentration with increasing depth, followed by a subsequent decrease. This suggests the existence of an optimal depth for DOC concentration, which is consistent with algae distribution with depth.

5.2. Biotic factors

In addition to abiotic factors, it is pertinent to examine the role of certain biotic factors in the dynamics evolution of DOC concentration. This subsection investigates the effect of different levels of parameters d_a, l_a, d_b, and l_b, which represent the metabolism rates of algae and bacteria.

We explore the effect of algal respiration and mortality on carbon sequestration. As illustrated in Fig. 5.19, when l_a is low (e.g., $l_a = 0.01$), an increase in d_a initially leads to a rise followed by a decline in DOC concentration (see Fig. 5.20(a)). This pattern arises because substantial organic matter accumulates within the algae when the respiration rates are at low levels. Consequently, the low death rate of algae promotes the exudation of organic matter, thereby increasing DOC concentration. However, as the death rate continues to increase, algal biomass decreases, resulting in reduced carbon sequestration and a subsequent decline in DOC concentration. Conversely, when $l_a = 0.08$, DOC concentrations decrease with a rising death rate (see Fig. 5.20(b)).

We then examine the impact of bacterial respiration and mortality on carbon sequestration, as depicted in Fig. 5.21. When d_b keeps constant, an increase in l_b decreases DOC concentration. This phenomenon occurs because an elevated bacterial respiration rate diminishes bacterial biomass, reducing DOC consumption. Consequently, a high bacterial respiration rate promotes carbon sequestration. However, when l_b is fixed (e.g., $l_b = 0.4$), even though a high bacterial death rate reduces bacterial biomass and lowers DOC consumption, DOC concentration decreases. This is attributed to the high death rate resulting in decreased bacterial biomass and thus reducing DOC recycling from bacteria. Consequently, a high bacterial death rate diminishes carbon sequestration.

6. Discussion

Numerous ecological stoichiometry models have been developed to analyze the effects of multiple elements on ecological interactions in an intricate way. However, these models assume that the system is entirely open to carbon, limiting their applicability in investigating the potential consequences of elevated atmospheric carbon dioxide concentration on food webs. This limitation arises because carbon availability for photosynthesis is not adequately represented. Many studies

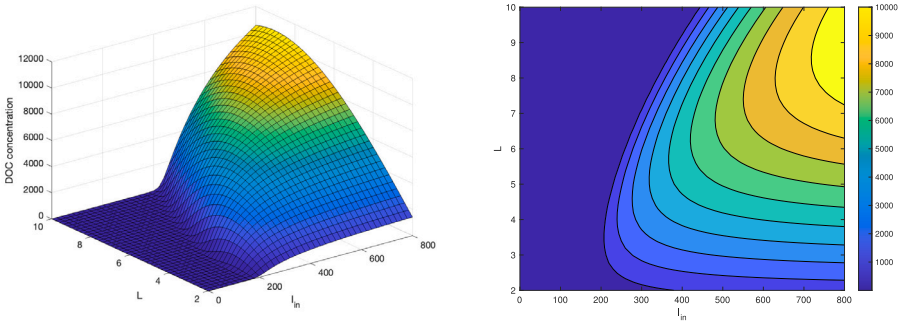

Fig. 5.18. Bifurcation surface and contour plot of DOC concentration for $I_{in} \in (0, 800)$ and $L \in (2, 10)$.

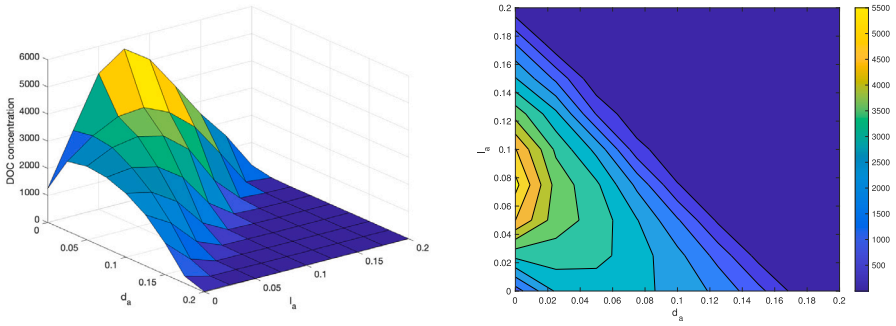

Fig. 5.19. Bifurcation surface and contour plot of DOC concentration for $I_a \in (0, 0.2)$ and $d_a \in (0, 0.2)$.

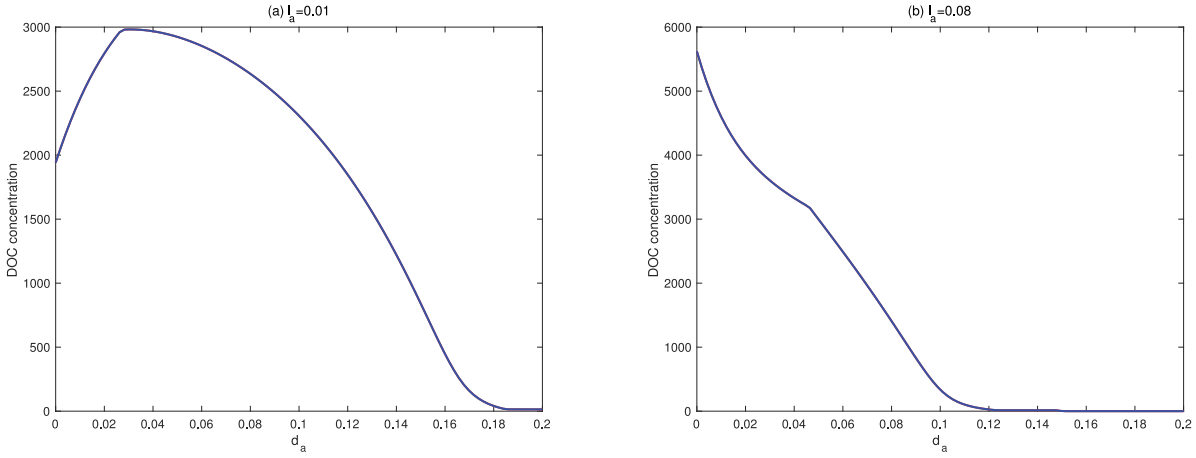

Fig. 5.20. Bifurcation diagrams of DOC concentration with d_a being the bifurcation parameter. Here $I_a = 0.01$ (left) and $I_a = 0.08$ (right). Other parameters are taken from Table 2.2.

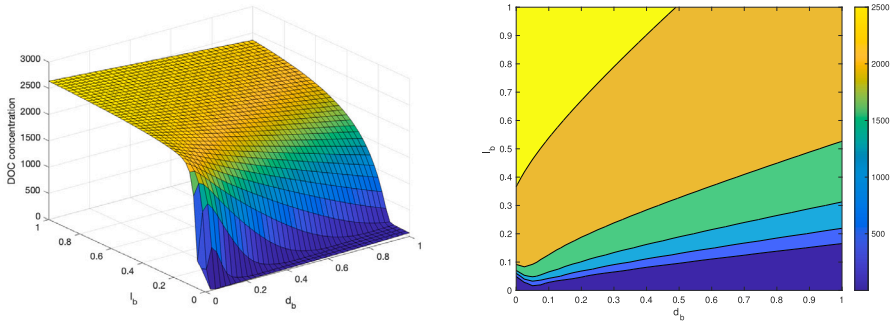

Fig. 5.21. Bifurcation surface and contour plot of DOC concentration for $I_b \in (0, 1)$ and $d_b \in (0, 1)$.

have demonstrated that an upsurge in atmospheric carbon dioxide can enhance the rate of photosynthesis, leading to a corresponding increase in the growth and production of autotrophs [53]. In algae-bacteria systems affected by elevated carbon dioxide, the resulting elevation in organic carbon concentration and reduction in nutrient levels can significantly impact the growth of bacteria.

To explore the potential consequences of the ongoing global rise in atmospheric carbon dioxide on algae-bacteria systems, we formulate a novel stoichiometric model that explicitly accounts for inorganic carbon availability. Based on [9], the model considers light, nutrients, and carbon dioxide as limiting factors for algae growth, while organic carbon and nutrients restrict bacterial growth. Furthermore, the model explicitly incorporates the generation and consumption of carbon dioxide, allowing for some degree of openness in the system concerning carbon.

The whole system exhibits a biologically significant forward invariant region, rendering the system dissipativity. A simplified scenario of the model, where B is set to be zero, was scrutinized. In this specific scenario, a threshold is established for the death rate of algae. Additionally, sufficient conditions are derived for the global asymptotic stability of the nutrient-only steady state, contingent on various parameters such as total phosphorus input, carbon dioxide input, and water surface light intensity. Moreover, sufficient conditions are established for a positive steady state, unraveling the intricate stability conditions associated with this equilibrium. During the bifurcation analysis of the simplified case, several abiotic factors are scrutinized, including phosphorus input, inorganic carbon input, light intensity at the water surface, and water depth. These parameters are crucial limiting factors for algae growth.

In parallel to the algal threshold, we also introduce the bacterial survival threshold. Simulations were carried out to scrutinize the repercussions of potentially limiting parameters on the algae-bacteria system. Specifically, heightened phosphorus levels can promote the coexistence of algae and bacteria, given that phosphorus is a vital nutrient for the growth of both. Furthermore, bacteria face extinction at low R_{in} and I_{in} due to an insufficient quantity of organic carbon and at high R_{in} and I_{in} due to inadequate phosphorus availability.

Carbon sequestration holds significant importance as a response to climate change, aiming to mitigate the trend of global climate warming by absorbing and storing CO_2 from the atmosphere, thereby reducing the cumulative concentration of greenhouse gases. Several factors that affect carbon sequestration are deliberately considered. First, although eutrophication encourages algal growth and can lead to algal blooms, it ultimately diminishes carbon sequestration. Similarly, an increase in light intensity yields a comparable outcome. Furthermore, elevated atmospheric CO_2 levels can potentially mitigate eutrophication in water bodies. Additionally, our exploration of the metabolism rates of algae and bacteria reveals that a high algal respiration rate correlates with a decrease in DOC concentration, whereas a high bacterial respiration rate facilitates carbon sequestration.

The model formulation and analyses still have certain limitations. The model is built on the assumption of independent co-limitation of algae growth by carbon, light, and phosphorus. Although there is evidence supporting independent colimitation by carbon and phosphorus [54], conclusive evidence for colimitation of algae growth by light and carbon is lacking. In addition, the model does not account for various effects of carbon dioxide on algae. Apart from promoting algal photosynthesis, carbon dioxide can decrease water pH, potentially reducing algae productivity [55], which is absent in our modeling. Additionally, atmospheric carbon dioxide concentration exhibits noticeable periodicity, with lower levels in summer and higher levels in winter. Therefore, it is reasonable and realistic to incorporate such seasonal variations into the subsequent modeling studies.

What is more, the algae considered are autotrophic in this study. However, mixotrophy, which combines autotrophic and heterotrophic nutrition, is a critical trophic strategy in planktonic microbes [56–58]. This dual strategy plays a significant role in maintaining carbon and nutrient cycles, enhancing ecosystem productivity and stability, and supporting the biological carbon pump by efficiently transferring energy and nutrients through the food web [59]. Hence, understanding the degree of mixotrophy in algae will be crucial and interesting for future research on the interactions between algae and bacteria.

Furthermore, autochthonous carbon, produced by algae, is the only source of DOC considered in the model. In contrast, the contribution of allochthonous carbon (i.e., the terrestrial inflow of organic matter to the water) is often significant in both freshwater and marine systems [60,61]. We have numerically explored the impact of terrestrial inflow of organic matter on the growth of bacteria and algae, but the results indicated that the external input of DOC did not significantly affect the growth of bacteria and algae. Consequently, determining how to incorporate the external input of DOC into our model more appropriately is also an important topic for future research. Finally, this model would benefit from data fitting and validation for enhanced reliability. Currently, many of the examined parameter regions are predominantly theoretical. Incorporating data from experiments such as free-air carbon enrichment and studies by Urabe et al. [18] would help identify parameter regions requiring further investigation.

CRediT authorship contribution statement

Zhenyao Sun: Writing – review & editing, Writing – original draft, Methodology, Conceptualization. **Hao Wang:** Writing – review & editing, Supervision, Conceptualization. **Meng Fan:** Writing – review & editing, Supervision, Conceptualization.

Declaration of competing interest

All authors declare no conflicts of interest in this paper.

Data availability

No data was used for the research described in the article.

Acknowledgments

Zhenyao Sun's research was supported by the National Natural Science Foundation of China (No. 12071068) and the China Scholarship Council (No. 202206620048). Hao Wang's research was partially supported by the Natural Sciences and Engineering Research Council of Canada (Individual Discovery Grant RGPIN-2020-03911 and Discovery Accelerator Supplement Award RGPAS-2020-00090) and the Canada Research Chairs program (Tier 1 Canada Research Chair Award). Meng Fan's research was partially supported by the National Natural Science Foundation of China (No. 12071068).

References

[1] K.W. Crane, J.P. Grover, Coexistence of mixotrophs, autotrophs, and heterotrophs in planktonic microbial communities, J. Theoret. Biol. 262 (3) (2010) 517–527, [Online]. Available: http://dx.doi.org/10.1016/j.jtbi.2009.10.027.
[2] H. Stickney, R. Hood, D. Stoecker, The impact of mixotrophy on planktonic marine ecosystems, Ecol. Model. 125 (2–3) (2000) 203–230.
[3] X. Chang, J. Shi, H. Wang, Spatial modeling and dynamics of organic matter biodegradation in the absence or presence of bacterivorous grazing, Math. Biosci. 331 (2021) 108501.
[4] J.P. Grover, The impact of variable stoichiometry on predator-prey interactions: a multinutrient approach, Amer. Nat. 162 (1) (2003) 29–43.
[5] J.D. Kong, P. Salceanu, H. Wang, A stoichiometric organic matter decomposition model in a chemostat culture, J. Math. Biol. 76 (2018) 609–644.
[6] M. Chen, M. Fan, R. Liu, X. Wang, X. Yuan, H. Zhu, The dynamics of temperature and light on the growth of phytoplankton, J. Theoret. Biol. 385 (2015) 8–19.
[7] K. Yoshiyama, H. Nakajima, Catastrophic transition in vertical distributions of phytoplankton: alternative equilibria in a water column, J. Theoret. Biol. 216 (4) (2002) 397–408.

[8] J. Zhang, J.D. Kong, J. Shi, H. Wang, Phytoplankton competition for nutrients and light in a stratified lake: a mathematical model connecting epilimnion and hypolimnion, J. Nonlinear Sci. 31 (2021) 1–42.

[9] H. Wang, H.L. Smith, Y. Kuang, J.J. Elser, Dynamics of stoichiometric bacteria-algae interactions in the epilimnion, SIAM J. Appl. Math. 68 (2) (2007) 503–522, [Online]. Available: http://dx.doi.org/10.1137/060665919.

[10] K.F. Edwards, Mixotrophy in nanoflagellates across environmental gradients in the ocean, Proc. Natl. Acad. Sci. 116 (13) (2019) 6211–6220.

[11] C. Körner, Biosphere responses to CO_2 enrichment, Ecol. Appl. 10 (6) (2000) 1590–1619.

[12] O. Hoegh-Guldberg, P.J. Mumby, A.J. Hooten, R.S. Steneck, P. Greenfield, E. Gomez, C.D. Harvell, P.F. Sale, A.J. Edwards, K. Caldeira, et al., Coral reefs under rapid climate change and ocean acidification, Science 318 (5857) (2007) 1737–1742.

[13] J. Zhang, C.J. Fischer, Carbon dynamics of Florida Bay: Spatiotemporal patterns and biological control, Environ. Sci. Technol. 48 (16) (2014) 9161–9169.

[14] S. Solomon, Climate Change 2007-The Physical Science Basis: Working Group I Contribution to the Fourth Assessment Report of the IPCC, vol. 4, Cambridge University Press, 2007.

[15] K. Gao, Y. Zheng, Combined effects of ocean acidification and solar UV radiation on photosynthesis, growth, pigmentation and calcification of the coralline alga Corallina sessilis (Rhodophyta), Glob. Change Biol. 16 (8) (2010) 2388–2398.

[16] M.J. Behrenfeld, R.T. O'Malley, D.A. Siegel, C.R. McClain, J.L. Sarmiento, G.C. Feldman, A.J. Milligan, P.G. Falkowski, R.M. Letelier, E.S. Boss, Climate-driven trends in contemporary ocean productivity, Nature 444 (7120) (2006) 752–755.

[17] X. Zhao, L. Liu, H. Wang, M. Fan, Ecological effects of predator harvesting and environmental noises on oceanic coral reefs, Bull. Math. Biol. 85 (7) (2023) 59.

[18] J. Urabe, J. Togari, J.J. Elser, Stoichiometric impacts of increased carbon dioxide on a planktonic herbivore, Glob. Change Biol. 9 (6) (2003) 818–825.

[19] R. Lal, Carbon sequestration, Phil. Trans. R. Soc. B 363 (1492) (2008) 815–830.

[20] A. Ortega, N.R. Geraldi, I. Alam, A.A. Kamau, S.G. Acinas, R. Logares, J.M. Gasol, R. Massana, D. Krause-Jensen, C.M. Duarte, Important contribution of macroalgae to oceanic carbon sequestration, Nat. Geosci. 12 (9) (2019) 748–754.

[21] L.J. Tranvik, J.A. Downing, J.B. Cotner, S.A. Loiselle, R.G. Striegl, T.J. Ballatore, P. Dillon, K. Finlay, K. Fortino, L.B. Knoll, et al., Lakes and reservoirs as regulators of carbon cycling and climate, Limnol. Oceanogr. 54 (6part2) (2009) 2298–2314.

[22] J.B. Cotner, B.A. Biddanda, Small players, large role: microbial influence on biogeochemical processes in pelagic aquatic ecosystems, Ecosystems 5 (2002) 105–121.

[23] S. Viswanaathan, P.K. Perumal, S. Sundaram, Integrated approach for carbon sequestration and wastewater treatment using algal–bacterial consortia: Opportunities and challenges, Sustainability 14 (3) (2022) 1075.

[24] R.W. Sterner, J.J. Elser, Ecological Stoichiometry: The Biology of Elements from Molecules to the Biosphere, Princeton University Press, 2003.

[25] X. Li, H. Wang, Y. Kuang, Global analysis of a stoichiometric producer–grazer model with holling type functional responses, J. Math. Biol. 63 (5) (2011) 901–932.

[26] I. Loladze, Y. Kuang, J.J. Elser, Stoichiometry in producer-grazer systems: linking energy flow with element cycling, Bull. Math. Biol. 62 (2000) 1137–1162.

[27] H. Wang, Y. Kuang, I. Loladze, Dynamics of a mechanistically derived stoichiometric producer-grazer model, J. Biol. Dyn. 2 (3) (2008) 286–296.

[28] I. Loladze, Y. Kuang, J.J. Elser, W.F. Fagan, Competition and stoichiometry: coexistence of two predators on one prey, Theor. Popul. Biol. 65 (1) (2004) 1–15.

[29] A. Peace, Effects of light, nutrients, and food chain length on trophic efficiencies in simple stoichiometric aquatic food chain models, Ecol. Model. 312 (2015) 125–135.

[30] X. Rong, Y. Sun, M. Fan, H. Wang, Stoichiometric modeling of Aboveground–Belowground interaction of herbaceous plant and two herbivores, Bull. Math. Biol. 82 (2020) 1–35.

[31] C.M. Davies, H. Wang, Incorporating carbon dioxide into a stoichiometric producer–grazer model, J. Math. Biol. 83 (5) (2021) 49.

[32] B. Boehrer, M. Schultze, Stratification of lakes, Rev. Geophys. 46 (2) (2008).

[33] D. Jiang, K. Lam, Y. Lou, Z. Wang, Monotonicity and global dynamics of a nonlocal two-species phytoplankton model, SIAM J. Appl. Math. 79 (2) (2019) 716–742.

[34] C.M. Heggerud, H. Wang, M.A. Lewis, Transient dynamics of a stoichiometric cyanobacteria model via multiple-scale analysis, SIAM J. Appl. Math. 80 (3) (2020) 1223–1246.

[35] J. Huisman, F.J. Weissing, Light-limited growth and competition for light in well-mixed aquatic environments: An elementary model, Ecology (2006) 507–520, [Online]. Available: http://dx.doi.org/10.2307/1939554.

[36] J.P. Grover, Resource competition and community structure in aquatic micro-organisms: experimental studies of algae and bacteria along a gradient of organic carbon to inorganic phosphorus supply, J. Plankton Res. 22 (8) (2000) 1591–1610.

[37] J.M.H. Verspagen, D.B. Van de Waal, J.F. Finke, P.M. Visser, E. Van Donk, J. Huisman, Rising CO_2 levels will intensify phytoplankton blooms in eutrophic and hypertrophic lakes, PLoS One 9 (8) (2014) e104325, [Online]. Available: http://dx.doi.org/10.1371/journal.pone.0104325.

[38] D.B. Van de Waal, J.M. Verspagen, J.F. Finke, V. Vournazou, A.K. Immers, W.E.A. Kardinaal, L. Tonk, S. Becker, E. Van Donk, P.M. Visser, J. Huisman, Reversal in competitive dominance of a toxic versus non-toxic cyanobacterium in response to rising CO_2, ISME J. 5 (9) (2011) 1438–1450, [Online]. Available: http://dx.doi.org/10.1038/ismej.2011.28.

[39] Y. Yan, J. Zhang, H. Wang, Dynamics of stoichiometric autotroph-mixotroph-bacteria interactions in the epilimnion, Bull. Math. Biol. 84 (1) (2021) [Online]. Available: http://dx.doi.org/10.1007/s11538-021-00962-9.

[40] H. Nie, S.-B. Hsu, J.P. Grover, Algal competition in a water column with excessive dioxide in the atmosphere, J. Math. Biol. 72 (7) (2015) 1845–1892, [Online]. Available: http://dx.doi.org/10.1007/s00285-015-0926-8.

[41] F.R. Vasconcelos, S. Diehl, P. Rodríguez, P. Hedström, J. Karlsson, P. Byström, Asymmetrical competition between aquatic primary producers in a warmer and browner world, Ecology 97 (10) (2016) 2580–2592, [Online]. Available: http://dx.doi.org/10.1002/ecy.1487.

[42] S. Diehl, S. Berger, R. Wöhrl, Flexible nutrient stoichiometry mediates environmental influences, on phytoplankton and its resources, Ecology 86 (11) (2007) 2931–2945, [Online]. Available: http://dx.doi.org/10.1890/04-1512.

[43] H.R. Thieme, Convergence results and a Poincaré-Bendixson trichotomy for asymptotically autonomous differential equations, J. Math. Biol. 30 (7) (1992) 755–763, [Online]. Available: https://doi-org.login.ezproxy.library.ualberta.ca/10.1007/BF00173267.

[44] X.-Q. Zhao, Dynamical Systems in Population Biology, Springer, New York, 2003, [Online]. Available: https://doi-org.login.ezproxy.library.ualberta.ca/10.1007/978-0-387-21761-1.

[45] L. Perko, Differential Equations and Dynamical Systems, vol. 7, Springer Science & Business Media, 2013.

[46] F. Azam, T. Fenchel, J.G. Field, J.S. Gray, L.-A. Meyer-Reil, F. Thingstad, et al., The ecological role of water-column microbes in the sea, Mar. Ecol. Prog. Ser. Oldendorf 10 (3) (1983) 257–263.

[47] C. Brussaard, G. Gast, F. Van Duyl, R. Riegman, Impact of phytoplankton bloom magnitude on a pelagic microbial food web, Mar. Ecol. Prog. Ser. 144 (1996) 211–221.

[48] R.G. Wetzel, Limnology: Lake and River Ecosystems, gulf professional publishing, 2001.

[49] Z. Jiang, S. Liu, J. Zhang, Y. Wu, C. Zhao, Z. Lian, X. Huang, Eutrophication indirectly reduced carbon sequestration in a tropical seagrass bed, Plant Soil 426 (2018) 135–152.

[50] H. Xu, H.W. Paerl, B. Qin, G. Zhu, G. Gaoa, Nitrogen and phosphorus inputs control phytoplankton growth in eutrophic Lake Taihu, China, Limnol. Oceanogr. 55 (1) (2010) 420–432.

[51] X. Liu, H. He, Z. Liu, Effects of CO_2 fertilization in aquatic ecosystems on the carbon sequeatration and eutrophication mitigation, Quat. Sci. 43 (2) (2023) 573–585.

[52] N.J. Anderson, H. Bennion, A.F. Lotter, Lake eutrophication and its implications for organic carbon sequestration in Europe, Glob. Change Biol. 20 (9) (2014) 2741–2751.

[53] E.A. Ainsworth, A. Rogers, The response of photosynthesis and stomatal conductance to rising CO_2: mechanisms and environmental interactions, Plant Cell Environ. 30 (3) (2007) 258–270.

[54] E. Spijkerman, F. de Castro, U. Gaedke, Independent colimitation for carbon dioxide and inorganic phosphorus, PLoS One 6 (12) (2011) e28219.

[55] N. Bates, M. Best, K. Neely, R. Garley, A. Dickson, R. Johnson, Detecting anthropogenic carbon dioxide uptake and ocean acidification in the North Atlantic Ocean, Biogeosciences 9 (7) (2012) 2509–2522.

[56] R.I. Jones, Mixotrophy in planktonic protists: an overview, Freshwater Biol. 45 (2) (2000) 219–226.

[57] K.F. Edwards, Mixotrophy in nanoflagellates across environmental gradients in the ocean, Proc. Natl. Acad. Sci. 116 (13) (2019) 6211–6220.

[58] F. Unrein, R. Massana, L. Alonso-Sáez, J.M. Gasol, Significant year-round effect of small mixotrophic flagellates on bacterioplankton in an oligotrophic coastal system, Limnol. Oceanogr. 52 (1) (2007) 456–469.

[59] A. Mitra, K.J. Flynn, J.M. Burkholder, T. Berge, A. Calbet, J.A. Raven, E. Granéli, P.M. Glibert, P.J. Hansen, D.K. Stoecker, et al., The role of mixotrophic protists in the biological carbon pump, Biogeosciences 11 (4) (2014) 995–1005.

[60] M. Bastidas Navarro, L. Schenone, N. Martyniuk, E. Vega, B. Modenutti, E. Balseiro, Predicting dissolved organic matter lability and carbon accumulation in temperate freshwater ecosystems, Ecosystems 25 (4) (2022) 795–811.

[61] D. Figueroa, O. Rowe, J. Paczkowska, C. Legrand, A. Andersson, Allochthonous carbon-a major driver of bacterioplankton production in the subarctic Northern Baltic Sea, Microb. Ecol. 71 (2016) 789–801.